Broadband Reflectivity and Emissivity Engineering Using Patterned Surfaces

by

AMIN BALAZADEH KOUCHEH

Submitted to the Graduate School of Natural Science and Engineering

In partial fulfillment of

the requirement for the degree of Master of Science

Sabanci University

December 2021

Broadband Reflectivity and Emissivity Engineering Using Patterned Surfaces

APPROVED BY:

DATE OF APPROVAL:

ABSTRACT

Broadband Reflectivity and Emissivity Engineering Using Patterned Surfaces

AMIN BALAZADEH KOUCHEH

Mechatronics Engineering, M.S. Thesis, December 2021

Thesis Supervisor: Prof. Dr. İbrahim Kürşat Şendur

Keywords: Spectral reflection; broadband reflectivity; thin-film coatings; impedance mismatch method; Inverse design method.

Optical coatings composed of thermomechanically superior materials with high reflectance in the broadband spectrum have recently attracted attention. Tungsten (W), among other refractory metals, suits well for applications that require high thermomechanical stability but suffer from low reflectivity below 1.5 μm. This thesis aims to propose design methods to optimize patterned multi-layer nanostructures that lower Tungsten's absorption over a broadband spectrum.

The first proposed design mimics the patterns observed on Morpho butterfly wings and increases the reflectivity of W over a broad spectrum. At the initial stage, the impedance mismatch method is implemented to optimize the number and thickness of the homogeneous multi-layers over the broadband spectrum. Then, the proposed pattern is incorporated into the homogenous structure. For the second structure, after optimizing the thickness and number of SiO_2/TiO_2 layers stacked on Tungsten as the initial design, the inverse design approach is utilized to construct holes that increase reflectivity in the dip points caused by interference effects.

Different design parameters are studied for both structures, the origin of optical phenomena is explained, and the effect of fabrication impurities is taken into account. The proposed structures and methods can be used in various optical applications.

ÖZET

Desenli Yüzeyler Kullanarak Geniş Bant Yansıma ve Yayımlılık Mühendisliği

AMIN BALAZADEH KOUCHEH

Mekatronik Mühendisliği YÜKSEK LİSANS TEZİ, Aralık 2021

Tez Danışmanı: Prof. Dr. İbrahim Kürşat Şendur

Anahtar Kelimeler: Spektral yansıma, Geniş bant yansıtma özelliği, Ince filim kaplama, Empedans uyumsuzluk metodu, Tersine tasarım yaklaşımı

Geniş bant spektrumunda yüksek yansıtma özelliğine sahip termomekanik olarak üstün malzemelerden oluşan optik kaplamalar son zamanlarda dikkat çekmiştir. Tungsten (W), diğer VIB grubu malzemeleri arasında, yüksek termomekanik kararlılık gerektiren uygulamalar için uygundur ancak 1,5 μm'nin altında düşük yansıtıcılığa sahiptir. Bu tez, geniş bantlı bir spektrumunda Tungsten'in absorpsiyonunu azaltan desenli çok katmanlı Nano yapıları optimize etmek için tasarım yöntemleri önermeyi hedeflenmektedir. Önerilen ilk tasarım, Morpho kelebek kanatlarında gözlemlenen desenlerden ilham almıştır, ve geniş bir spektrumda W'nin yansıtıcılığını arttırır.

Birinci aşamada, geniş bant spektrumu üzerinde homojen çok tabakaların sayısını ve kalınlığını optimize etmek için empedans uyumsuzluk yöntemi uygulanmıştır. Daha sonra önerilen desen homojen yapıya dahil edildi. İkinci yapı için, ilk tasarımda Tungsten üzerine yığılmış SiO2/TiO2 katmanların kalınlığı ve sayısı optimize edildikten sonra girişim etkilerinin neden olduğu dip noktalarında yansımayı arttıran delikler oluşturmak için tersine tasarım yaklaşımı kullanılmıştır.

Her iki yapı için de farklı tasarım parametreleri incelenmiştir. Optik fenomenlerin kökeni açıklanmıştır ve imalattan kaynaklı safsızlıkların etkisi hesaba katılmıştır. Önerilen yapılar ve yöntemler çeşitli optik uygulamalarında kullanılabilir.

ACKNOWLEDGEMENTS

During my MS degree at Sabanci University, where I have spent more than two years, I had the chance to meet great people to exchange ideas and collaborate with. Here, I want to express my sincerest gratitude for the great support and all the inspiring moments.

The persons I would like to start with are Mahyar Ghavami and Shahriar Rahbar. I owe a lot for their motivational words and guiding me to pursue my academic journey at Sabanci.

I would like to thank my supervisor Professor Kursat Sendur for his supervision, guidance, patience, and endless support. I consider myself very fortunate for the opportunity to be his student. Beside his academic achievements, his personality has been inspiring for me.

My sincerest gratitude also goes to Sabanci University (SU), Faculty of Engineering and Natural Science (FENS), and its staff for providing excellent research equipment and environment.

I would like to thank Dr. Ali Kecebas for what I have learned from him.

I want to express my gratitude to Dr. Eesa Rahimi and Dr. Armaghan for sharing their knowledge and allowing me to contribute to their projects.

I would like to thank Niloufar Pirouzfam for the tremendous amount of scientific conversation we had.

I want to thank Mirvahid Mohammadpour, Peiman Khandar, and Taha Behrouzi, who were always there.

I want to thank all of my lovely friends, especially Ali Shafaghi and Niloufar, Seyed Ali and Asal, Behanam and Darya, Mohammad Jafarpour, Milad and Kosar, Farid, Soroush, Taher, Reza, Sasan, Mohammad Joudivand, Sina, Kuray, and Mandana, who made a memorable and excellent environment at Sabanci.

I would like to thank my beloved family for all the inspiration, unconditional support throughout my lifetime. They have always encouraged me to follow my dreams. Without their support, guidance, and encouragement, this thesis would not have been possible.

This thesis is dedicated to my beloved family

TABLE OF CONTENTS

LIST OF FIGURES

LIST OF TABLES

1 INTRODUCTION

1.1 Background and Motivation

Research on broadband spectral reflection and absorption has attracted increasing attention recently due to the wide range of applications in both science and industry. Extensive literature in broadband radiative cooling systems [1–7], solar absorbers [8,9], broadband anti-reflectors [10,11], space applications [12,13] points out the importance of this issue. Various techniques were proposed in the literature to increase broadband spectral reflectance. One of the most common ways to achieve a high broadband optical reflection is to manipulate materials with inherent high reflective properties. Noble metals, including Au, Ag, and Cu, are considered the best candidates with broad spectral bandwidth [14]. Despite their ability to reflect the visible and near-infrared radiation over a broadband spectrum, other considerations such as thermal stability, low melting points, low Young's modulus, and high cost prevent them from being used in most broadband applications [15]. Refractory metals, such as tungsten, molybdenum, niobium, and tantalum, have been suggested to overcome these issues due to their superior thermomechanical properties [16]. As a group, they provide unique characteristics such as excellent strength at high temperatures, a high melting point, good resistance to corrosion, and high resistance to thermal shock, making them useful in harsh conditions [17]. The reflectivity and absorptivity of these metals can be seen in Fig. 1.

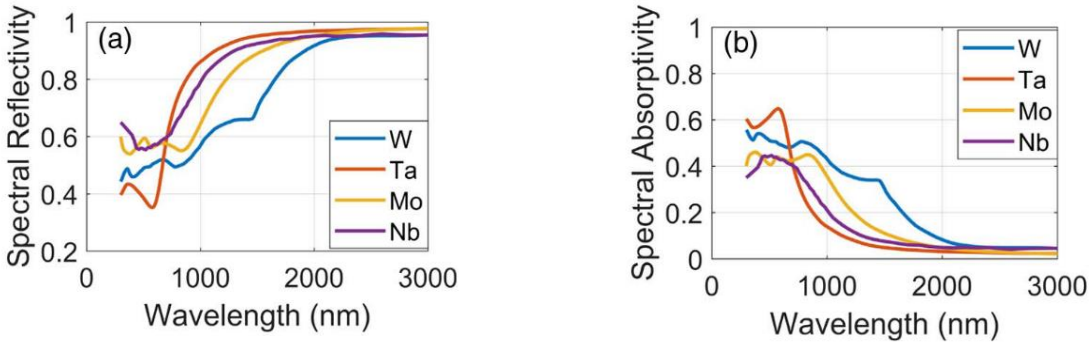

Figure. 1 a) Reflectivity, b) Absorptivity of refractory metals in 300-3000nm [18]

As it is clear from Fig1., despite these advantages, their reflectivity at shorter wavelengths is low. For instance, Tungsten has an average reflectivity of 95% in the wavelength range of 1500-3000nm, whereas its reflectivity drops to an average of 40-50% in the shorter wavelengths of 300-1500nm [18]. To come up with this issue, employing dielectric multi-layer thin-film coatings has been utilized recently as broadband reflectors that enhance reflectivity in shorter wavelengths [18,19]. Their promising results have prompted researchers to focus more on the geometry and material aspect of these coatings.

In terms of structure, coatings can be classified as homogeneous or inhomogeneous. Inhomogeneous coatings are scattered on the surface either randomly or in a pattern, whereas homogeneous coatings are often in the form of films that cover the whole surface. In general, the collective responses of multilayer films modify the spectral response of the surfaces on which they are coated. The phases of resultant waves from the interaction of incident waves with individual layers can be changed by varying layer thicknesses. These waves, which have various phases, can constructively or destructively interfere with one other. The primary mechanism that alters the spectral response of the structures is interference effects. Based on these interference effects, highly reflecting, narrowband, or broadband filters can be built.

On the other hand, inhomogeneous coatings are not multilayer structures in general, and interference effects are not the primary mechanism underlying their responses. Inhomogeneous structures are usually coated with a periodicity on the surface to trigger specific resonance modes. They are ideal for narrowband applications that require specialized spectral properties due to their resonant nature. The bandwidth or center wavelength of the resonance modes can be modified by adjusting the periodicity or pattern geometry.

Coatings' thermomechanical qualities, in addition to their spectral features, are significant depending on the working conditions. Once the wavelengths of interest are known, both homogeneous and inhomogeneous coatings can be developed for optical/thermal applications. Coating design and analysis are critical in broadband reflectance using refractory materials and high-temperature broadband thermal emitters. Different spectral properties in the broadband spectrum are required for each of these applications. Due to the working circumstances, material constraints also come into play in constructions with refractory metals and high-temperature broadband thermal emitters. Even though various research on these topics has been published in the literature, specific issues still need to be addressed. In this dissertation, design and analysis

methods for selected applications using both homogeneous and inhomogeneous filters are developed and evaluated, with material requirements also considered. The strategies proposed throughout the dissertation have been shown to be effective answers to the difficulties under consideration and can be applied to various coating design issues.

1.2 Literature Survey

This section contains relevant literature for the problems mentioned in the preceding section. The literature survey identifies the gaps in the literature and describes feasible solutions, which are investigated in this dissertation.

1.2.1 Enhancing Broadband Reflectivity Using Bio-Inspired Multilayer Structures

The optical nanostructure of insects has inspired researchers to design and optimize multi-layers. Among these insects, Morpho butterflies are known for their excellent multifunctional features of photonic structure wings [20]. These morphologies have been applied to the design and fabrication of bio-inspired sensors such as thermal infrared and PH sensors [21],[22], chemical sensors [23],[24], gas sensors [25], robotic tactile sensors [26], and acoustic sensors [27] alongside with applications in microfluidics [28],[29] and radiative cooling technology [30–32]. The multi-layered thin-film nanostructure wings of morpho butterflies play an important role in controlling the reflectivity of light. Researchers optimized Morpho butterflies' wing structure in several studies to increase reflectivity in the narrowband spectrum. The literature results demonstrate that alternating the number of layers, the distance between the layers and, the shape and thickness of the layers not only impact reflectivity but also are responsible for the wide-angle reflectance [33–38]. As indicated in the literature, increasing the number of layers and reducing the distance between the ridges increases reflectivity [39],[40]. In addition to the structure morphology, coating materials can also affect reflectivity. For instance, researchers have used the periodic arrangement of high/low index thin film layers to tune the spectral reflectivity of morpho butterfly-like structures [1,18,41].

Previous research also shows that the periodic structure of morpho butterfly wings helps them have lower wing temperatures. This indicates that the ridge distances between periodic structures enhance convection from the wings to the ambient air, which decreases the thermal stress on the wing nanostructure. This thermal/heat transfer property of the morpho butterfly wing's

nanostructure has been implemented to reduce the thermal load on the multi-layered structures [30,42].

Previous research on morpho butterflies' structures has concentrated on the narrowband spectrum. The purpose of the thesis is to fill out this gap by using optimization tools and combining them with the morpho butterfly's wing nanostructure to achieve broadband spectrum reflectivity. To date, developments in numerical methods have opened up numerous approaches to optimizing multi-layer thin-film coatings' structure. Implementing the genetic algorithm [43,44], needle optimization technique [45,46], evolutionary algorithm [3], and deep learning algorithms [47,48] to design film structures are some of the well-known methods.

By benefiting from those methods, multi-layers that mimic the geometry of the observed patterns in nature can be designed. By doing so, the advantages of structures that already exist in nature can be coupled to artificial structures.

1.2.2 Enhancing Broadband Reflectivity Using Topology Optimization

Both geometry and physical properties of materials are the principal elements to design nanophotonic devices. In this regard, comprehensive research is required to optimize and obtain the objectives by implementing numerical approaches. One of the well-known methods to engineering the geometry of the structures is the inverse design method. The main idea for the inverse design, which is known as topology optimization either, refers to recent decades, where it has been used in the field of mechanics to optimize the geometry by satisfying all constraints, and design variables enable the structure to bear the same amount of load [49]. In the earlier decades, enhancing the functionality of optical devices by increasing complex geometric design [50] along with developments in the field of optics/photonics and its structure related applications like extreme dielectric confinement structures [51], caused researchers to investigate more on the structure of optical devices by utilizing inverse design formulation in nanophotonics.

As expected from its name, the structure is unknown in an inverse design problem. Accordingly, an initial structure will be assumed to achieve a desired electric field and functionality at the first step. Then it will change through iterations until the required functionality with the final structure is obtained. The inverse design method can be categorized into different types, including heuristic [52-53], gradient-based [54-55], and the adjoint method [56-57]. Among all methods, using the adjoint approach to calculate the gradient efficiently, with two simulations per iteration, enables

the creation of designs in a significantly faster time frame, making this approach most advantageous. The benefits of this strategy have convinced researchers to utilize it widely in various applications of optics/electromagnetics such as nonlinear devices [58]. Although employing this method to design broadband high-temperature thermal emitter/absorber [59], broadband polarization intensive metamaterial perfect absorber [60], and broadband photonic crystal waveguide [61] demonstrates the ability of this approach to exploit in the broadband spectrum, utilizing this method in broadband reflectivity applications does not get enough attention in the literature up to now. Therefore, this thesis aims to solve this problem by using the inverse design method on a multilayer thin film coating.

1.3 Aims and Objectives

The main goal of this thesis is to engineer the spectral properties of surfaces using broadband engineering techniques. Tungsten, as one of the refractory metals, is of particular interest for applications requiring long-lasting coatings in harsh environments. Although durable coatings made of such materials are being investigated for high emission/absorption, broadband reflectors made of such materials have received little attention. Broadband reflectors like these are necessary for applications where incident radiation absorption causes substantial thermal stresses. The construction of refractory metal coatings with excellent broadband spectrum reflection is investigated here to meet this need.

To do this, first, we use a bio-inspired multi-layer structure to increase the broadband reflectance of Tungsten in a broadband spectrum. Layer thicknesses of homogenous thin-film structures with predetermined layer numbers and materials are optimized such that impedance mismatch between the structure and incident medium is maximized to achieve broadband reflectivity. To benefit from the thermal advantages of the morpho butterfly wings-like structures [30,39,42,62,63], spectral characteristics of such structures are studied by introducing periodicity, transforming homogenous multi-layers to inhomogeneous structures. In the second part, after optimizing the thickness and number of the SiO_2/TiO_2 thin film layers stacked on Tungsten, the effect of periodic holes on the reflection of the structure is analyzed to propose an initial design model for the inverse design calculations. Then, by finding the origin of dip points, the inverse design method is utilized to enhance reflectivity at those spectra.

Final structures exhibit very high, reaching up to 90 % levels, broadband reflectance in 0.3-3 μm spectra, which prevents the absorption of incident radiation from high-temperature sources in these spectrums and leads to increased thermomechanical stability.

1.4 Contributions

The presented thesis contributes to engineering and controlling the reflectivity/emissivity of surfaces, one of the optics/photonics branches. In particular, it includes unique design techniques for optical coatings that enable high broadband reflectivity.

Individual periodic high-low index layers are constructed at different wavelengths and stacked together to generate high reflection in the broadband spectrum. Broadband reflection is possible across the spectrum due to the low destructive interference of the reflected beams at the front surface. Although sharp peaks at different wavelengths can be seen throughout the spectrum, they do not result in a reduction in the reflection in the broadband spectrum. The underlying mechanics of the sharp peaks can be explained by defining the -S parameter. The influence of material properties on reflection is also investigated. Using the patterned/topological optimized models enhances the thermo-mechanical stability of the proposed structures. All in all, this research provides structures with an extremely high broadband reflection that may be employed in radiative cooling systems or space applications.

A scientific paper is published as an outcome of the first part of this research, and another is about to prepare for the second part.

- Koucheh, A. B., Kecebas, M. A., & Sendur, K. (2021). Impedance mismatch-based enhancement of broadband reflectance of tungsten with bio-inspired multilayers. *Journal of Quantitative Spectroscopy and Radiative Transfer*, *276*, 107899.

2 IMPEDANCE MISMATCH-BASED ENHANCEMENT OF BROADBAND REFLECTANCE OF TUNGSTEN WITH BIO-INSPIRED MULTILAYERS

2.1 Problem Definition

Elevated temperatures in the systems lead to a reduction in both device performance and lifetime. Refractory metals like W, Ta, Mo, and Nb are widely utilized in such high-temperature applications not only for their higher melting points but also for their superior mechanical characteristics, which make them less vulnerable to corrosion and mechanical damage [17]. However, those metals suffer from low reflectivity in visible and near-infrared spectrums, 0.3 – 1.5 μm wavelength interval, at which thermal radiation from high-temperature sources is strong, as depicted in Fig. 2(a).

In Fig. 2(a), thermal radiation from the sun (obtained by thermal blackbody radiation from a surface at 5850 K and with a solid angle of 6.84×10^{-5} at a perpendicular angle of incidence. The reflectivity of the W is also plotted with respect to wavelength in Fig. 2(a). The spectral distribution of absorbed power is also depicted in Fig. 2(b) together with the incident thermal radiation. The red-shaded region corresponds to absorbed radiation power with respect to wavelength, and the blue-shaded region represents the reflected power. Incident and absorbed powers are obtained by calculating the areas under these curves. In the interval of 0.3 – 1 μm interval (the red-shaded region in Fig. 2(a)), more than 1100 W/m^2 power reaches the atmosphere, and this power increases with reducing the distance to the sun. As seen from Fig. 2(a), the reflectivity of W is around 50 % levels which leads to absorption of nearly 600 W/m^2 of the incident power. At wavelengths longer than 1 μm (the green-shaded region in Fig. 2(a)), W has higher reflectivity reaching up to 90 % levels, preventing the absorption of incident thermal radiation at these wavelengths. Because of these spectral characteristics, the spectral reflectivity of refractory metals should be enhanced in the broadband spectrum for more efficient use in high-temperature applications such as aerospace [12-13].

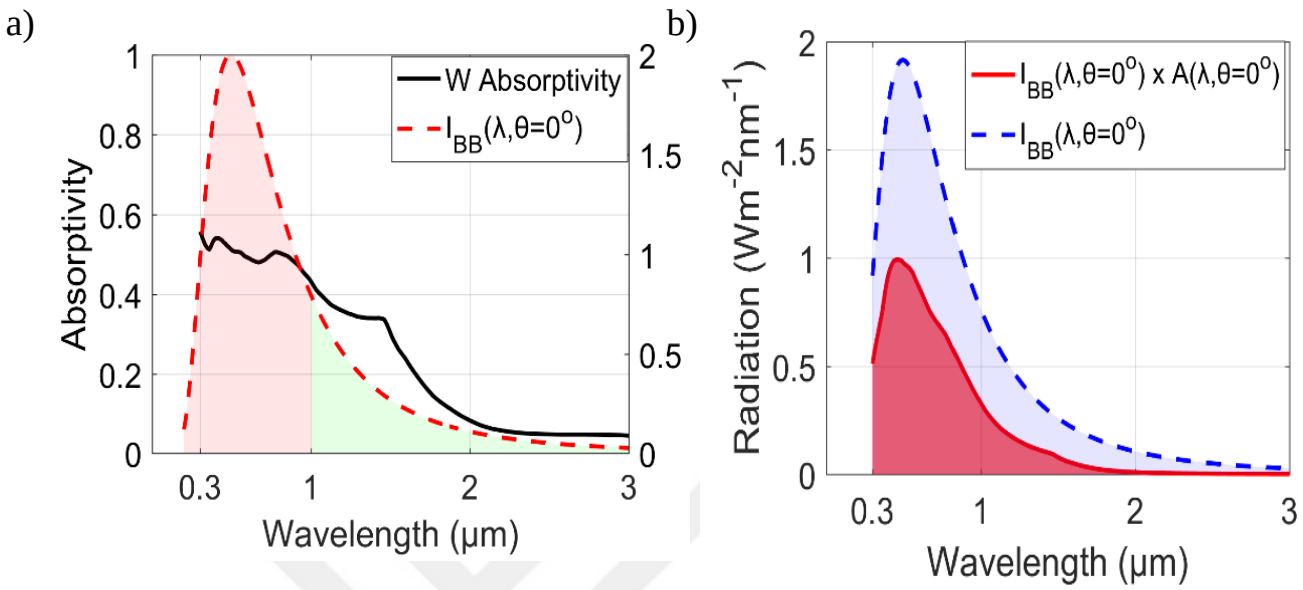

Figure 2. a) Spectral distribution of thermal radiation from the sun at a perpendicular angle of incidence and spectral reflectivity of W. b) Spectral distribution of thermal radiation from the sun at a perpendicular angle of incidence and absorbed power by -500 nm thick W layer.

2.2 Methodology

Among many other coating types, homogeneous multi-layer structures were previously reported to enhance the reflectivity of refractory metals [18, 64,65]. Despite their high reflectivity in the broadband spectrum, implementing a high number of layers causes fabrication difficulties in these types of coatings. In addition to homogeneous multilayers, the spectral characteristics of the patterns observed on the wings of the Morpho butterflies, which are composed of multilayer features separated from each other, are extensively studied [66]. However, such features were not utilized to enhance the spectral reflectance of refractory metals.

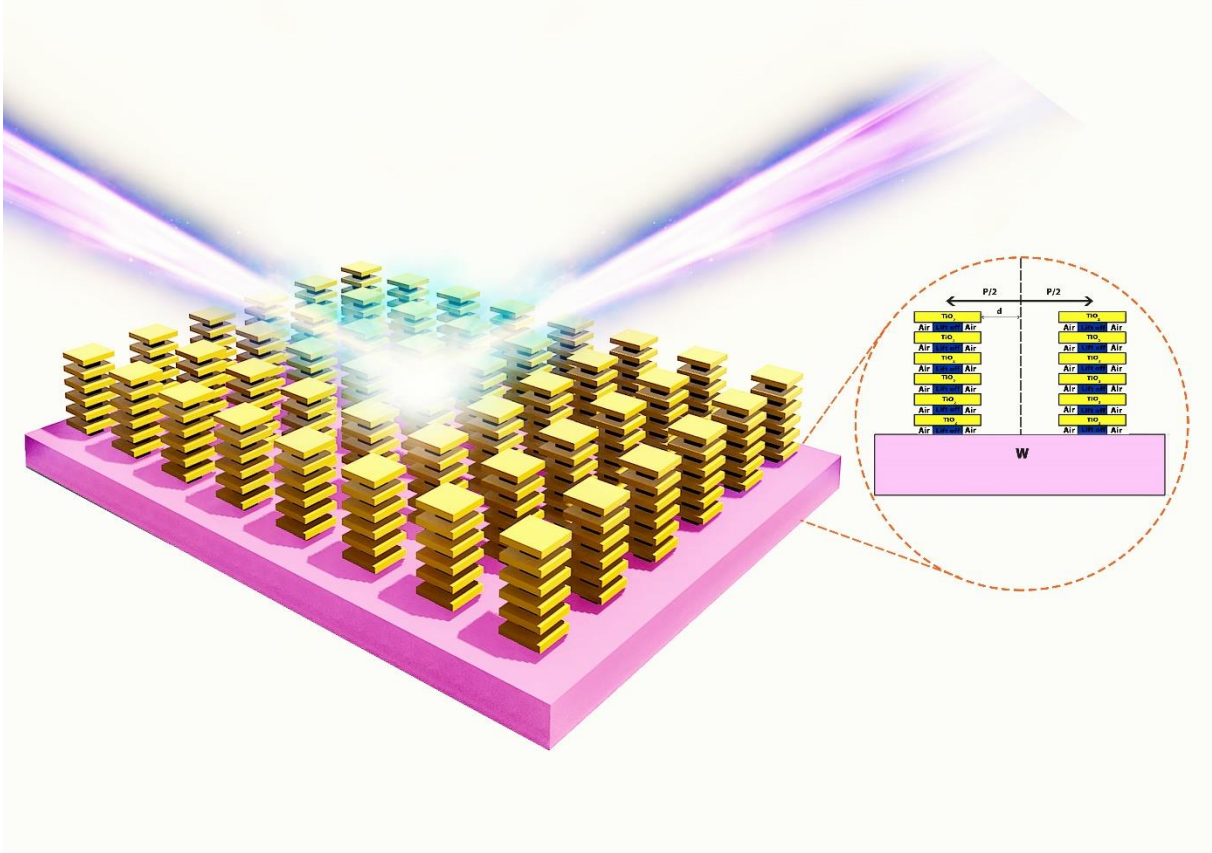

Figure 3. Schematic representation of multilayer structures inspired from wings of Morpho butterflies.

Besides, although the spectral reflectance of the periodic multilayer coatings inspired by Morpho butterfly wing's nanostructures is explored in a relatively narrowband spectrum so far, the effect of periodicity of the multilayers on the broadband reflectivity is not widely studied. Schematic representation of the structures in which inhomogeneities are introduced in transverse directions is visualized in Fig. 3. Based on the previous findings, which state that periodic arrangement of multilayers, inspired by the features on the wings of Morpho butterflies, would enhance the thermal management capability of the coatings [30,42].

The design of multi-layer structures with predetermined layer numbers and layer materials is studied in this work to address these issues and fill the gap in the related literature. First, spectral reflectance in 0.3 – 3 μm of the multi-layers composed of high-low index layers with a varying number of layers is optimized by tuning layer thicknesses. TiO_2 is chosen as high-index, and the air is selected as low index material. When excited with a plane wave, the incident wave encounters

TiO_2 layers separated by air gaps of varying thicknesses. Spectral reflectance of the structures is formulated based on the wave impedance approach, similar to the one used in [2], and optimization is conducted based on that formulation. When executed, the developed algorithm seeks a structure that maximizes the impedance mismatch between the substrate and the incident medium. Spectral characteristics of the resulting structures are both analyzed by wave impedance analysis and evaluating the total optical path that wave travels throughout the structure by summing individual optical thicknesses of the layers obtained by,

$$\delta_i = \frac{(2\pi n_i d_i)}{\lambda} \tag{1}$$

where δ_i is the optical thickness of the i^{th} layer, n_i is the refractive index of the medium/layer, d_i is the geometrical thickness, and λ is the wavelength.

As a next step, the effect of lift-off materials on the spectral reflectance of the multi-layers is studied. Lift-off materials are needed to realize the air gaps between TiO_2 layers. Finally, to study the effect of periodicity, multi-layers that do not have any inhomogeneities in transverse directions are transformed to structures depicted in Fig. 3, and their spectral reflectance is studied by FDTD [68]. In this case, the resulting reflectance spectrum characteristics are studied by obtaining the reflection coefficients/ *S* parameters of the studied multi-layers with different periodicities by an *S* parameters retrieval method for electromagnetic metamaterials [69].

2.2.1 Design of homogeneous multi-layers based on impedance mismatch

Starting from the intrinsic impedance of individual layers, which are solely dependent on material properties,

$$Z = \sqrt{\frac{\mu}{\varepsilon}} \tag{2}$$

and including the thicknesses of the layers and their interaction with each other, surface impedance of a multi-layer composed of *N* number of layers can be expressed as,

$$\mathcal{Z}_i = Z_i \frac{\mathcal{Z}_{i+1} + Z_i \tan(\delta_i)}{Z_i + j\mathcal{Z}_{i+1} \tan(\delta_i)} \tag{3}$$

From the surface impedance of a multi-layer structure, the amplitude of its reflectance coefficients and reflectance percentage is given as,

$$\Gamma = \frac{\mathcal{Z}_1/Z_0 - 1}{\mathcal{Z}_1/Z_0 + 1} \tag{4}$$

The reflectance coefficient values obtained by Eq. (4) at different wavelengths are schematized on a complex plane in Fig. 4(a). In Eq. (4), Z_0 is the intrinsic impedance of the air and is equal to 377 Ω and $\mathcal{Z}_1$ is the surface impedance of the multi-layer. By using Eqs. (2)-(4), reflection coefficients of a multi-layer structure and its reflectance, $R(\lambda) = |\Gamma(\lambda)|^2$ can be calculated. Since reflection coefficients are complex quantities, they are visualized on a complex plane, called the complex impedance plane/-S plane. An example distribution of complex reflection coefficients on the -S plane is represented in Fig. 4(a). It is observed that the reflection coefficients are distributed (green dots) inside a unit circle centered at the origin (blue circle). In Fig. 4(a), green dots correspond to reflection coefficients at different wavelengths, which always remain in the unit circle represented by blue color. This representation is very similar to the Smith chart [70] used in microwave and RF regimes for the purpose of impedance matching. From this representation, it is clear that zero reflectance at a wavelength is achieved only if the amplitude of the reflectance coefficient is zero, appears at the origin (red star). Since this condition is only satisfied if $Z_{Surf} = Z_0$, the origin of the unit circle is called a perfect impedance matching point. On the other hand, the magnitude of the reflectance coefficients on any point on the unit circle is always 1 ($|\Gamma| = |re^{i\theta}|, if\ r = 1$).

Therefore, any point on the unit circle is called a perfect impedance mismatch point. Based on these, the following can be deduced: Reflectance is reduced as the reflectance coefficient approaches the origin, and it increases as the reflection coefficient moves away from the origin. Such characteristics of the reflectance coefficients on the unit circle (S-plane) can be utilized to engineer the reflectance spectrum of the multi-layers. In Fig. 4(b), spectral reflectance of the tungsten substrate is shown, and corresponding reflectance coefficients are shown in Fig. 4(c). As seen from Fig. 4(c), W's reflectance is below 60 % at wavelengths shorter than 1 μm and starts to increase at longer wavelengths and reaches up to 95% levels.

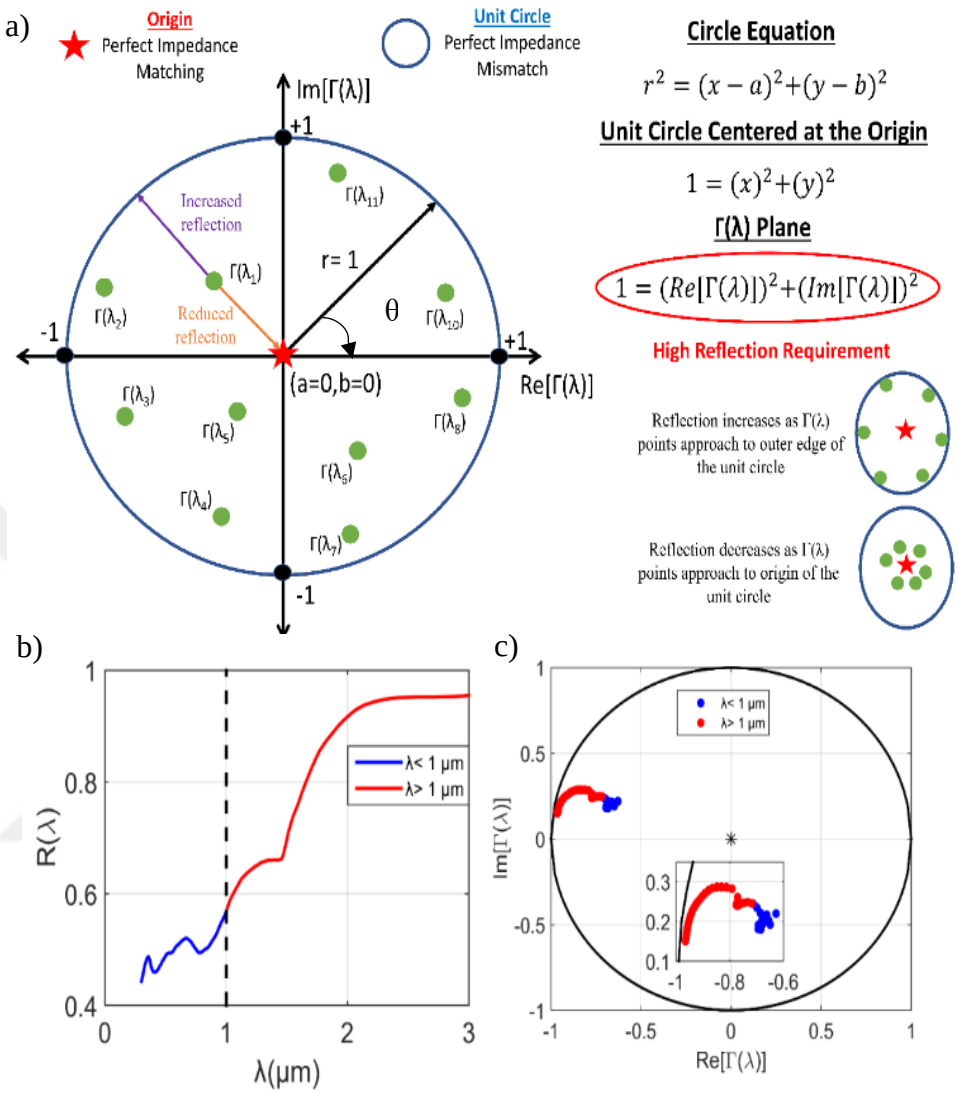

Figure 4. a) Representation of impedance mismatch method in -S plane. b) Reflectivity of W in 0.3 – 3 μm spectrum intervals. c) Reflection coefficients of W in -S plane.

Reflection coefficients of the low reflectance spectrum (blue points) are closer to the origin and start to approach the left side of the unit circle for longer wavelengths (red points). Here the aim is to preserve high reflectance at longer wavelengths while enhancing it in shorter wavelengths. Based on this, the design spectrum is separated as low and high reflectance spectrum, and a weighting is introduced in the mathematical expression of the problem and defined as,

$$max\ \alpha \int_{\lambda_1}^{\lambda_2} \left| r(\lambda) e^{i\theta(\lambda)} \right| d\lambda + (1-\alpha) \int_{\lambda_2}^{\lambda_3} \left| r(\lambda) e^{i\theta(\lambda)} \right| d\lambda \qquad (5)$$

where α is the weighting parameter, λ_1, λ_2, and λ_3 are 0.3, 1, and 3 μm respectively. α is chosen as 0.7 to keep the reflection reduction rate low at longer wavelengths while enhancing it at shorter wavelengths. Both homogenous and inhomogeneous structures' spectral characteristics are analyzed on the S-plane.

2.2.2 Analysis of introduced inhomogeneities in transverse directions

Effect of applied inhomogeneities in -x and -y directions on the spectral reflectance is obtained by FDTD [68] simulations. Periodic boundary conditions were used in -x and -y directions, PML boundary conditions were used in the z-direction. Studied multi-layer structures were excited with a -x polarized plane wave propagating in the z-direction. Realistic optical properties for TiO_2, obtained from [71], are used in all the calculations. Lift-off materials were used in FDTD simulations to analyze realizable multi-layers with a refractive index of 1.41, similar to one reported in [72], as well as for varying refractive indices and dimensions. Then a -S parameters retrieval method for metamaterials was used to obtain the -S parameters of the inhomogeneous multilayers [69]. Calculated -S parameters were used to analyze the spectral reflectance of the inhomogeneous multi-layers.

2.3 Results and Discussions

The average reflectance of the multilayer with the increasing number of layers is shown in Fig. 5(a), for which the corresponding layer materials and thicknesses are given in Table 1, and the spectral reflectance of the multilayer composed of eight layers is shown in Fig. 5(b). The average reflectance of the multilayer in both spectrum intervals reaches 95% levels from 50% and 80% levels for eight layers. Change of average also indicates that when layer number is higher than 4, there are enough design parameters to increase the average in both spectrum intervals. Amplitudes of the reflectance coefficients are also demonstrated in S-plane in Fig. 5(c). Illustrated amplitudes of the reflection coefficients of W with and without multi-layer agree with the spectral characteristics. As seen, all amplitude values shift towards the outer edge of the unit circle. Besides the broadband reflectance enhancement, a multi-layer structure yields sharp drops over the spectrum. To analyze the nature of the peaks and the broadband reflectance characteristics, the total optical path, δ_{Total}, that light travels throughout the homogeneous multi-layer structure, is plotted in Fig. 5(d).

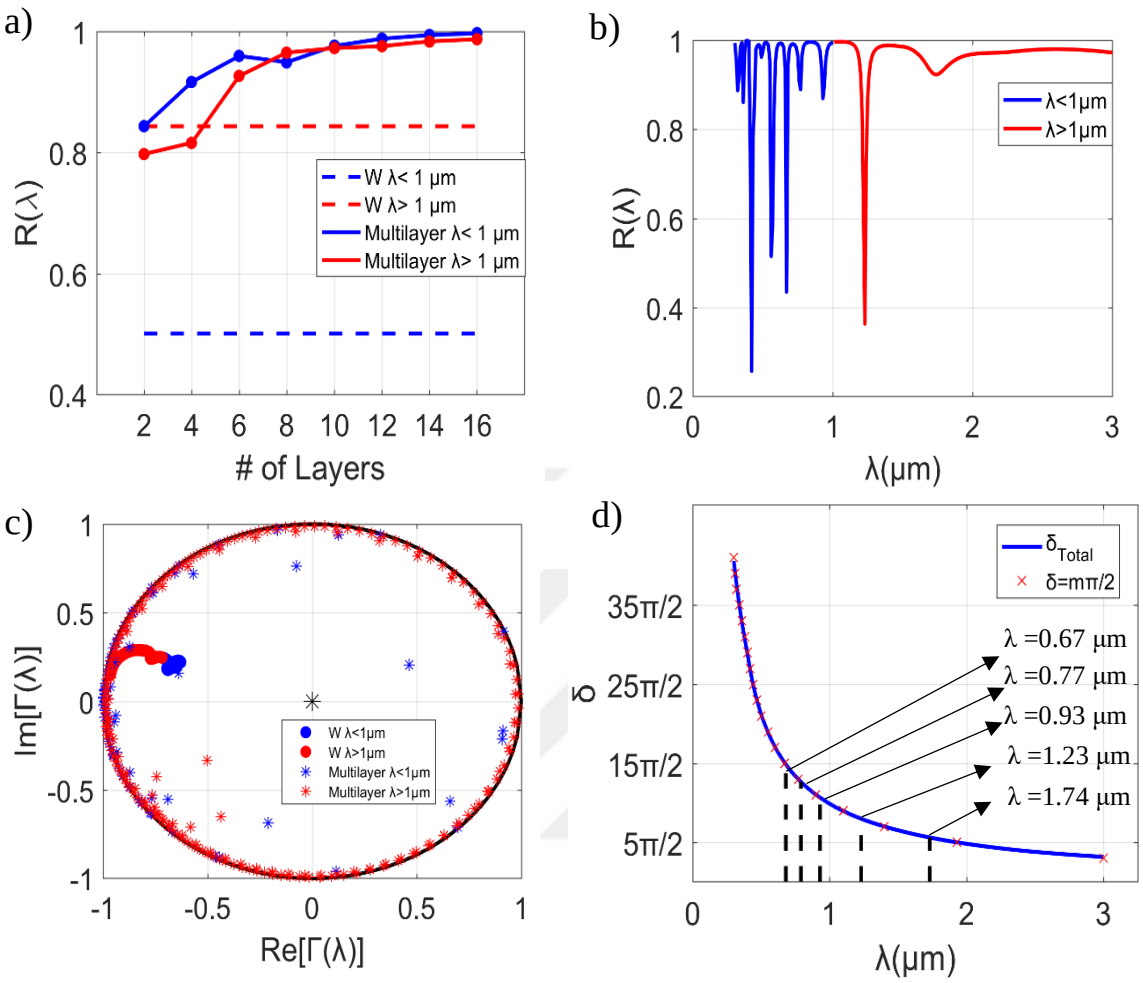

Figure 5. a) Reflectance of homogeneous multilayers for the increasing number of layers. b) Spectral reflectance of a multilayer with 8 layers designed for α =0.7 with TiO_2 and air. c) Reflectance coefficients of the multilayer whose spectral reflectance are shown in Fig. 5(b) on the -S plane. d) Comparison of optical thickness of the multilayer structure on which odd multiples are marked.

For verification purposes, we compared the reflectance spectrum of the 8-layered structure, for which layer materials and thicknesses are depicted in Table 1, obtained by the described impedance formulation, characteristic matrix method [73], and the FDTD [68]. As seen in Fig. 6(a), there is perfect agreement between the analytical solution (both impedance formulation and characteristic matrix method belong to this category) and the FDTD solution. Also, to quantify the dependence of the broadband reflectance spectrum on meshing, we compared the total absorption percentage, which is expressed as $I_{BB}(\lambda, T = 5850\ K)x\big(1 - R(\lambda)\big)x100/I_{BB}(\lambda, T = 5850\ K)$. As seen in Fig.

6(b), the absorption percentage remains around %8 and does not significantly change as the number of mesh points is increased beyond 14. Therefore, we proceeded with FDTD simulations with mesh points of 14.

Table 1. Thicknesses of the layers used in the multilayers with layer numbers of 2, 4, 6, 8, 10, 12, 14, and 16 on top of 500 nm W.

Layer Material	# of Layers							
	2	4	6	8	10	12	14	16
W (500 nm)	Thickness [nm]							
Air	119.15	106.2	279.04	268.94	62.43	88.35	185.98	59.1
TiO_2	67.04	68.28	93.08	256.86	126.53	220.75	680.19	181.23
Air		145.02	126.96	136.88	178	703.4	245.15	229.43
TiO_2		108.12	58	125.96	132.21	132.48	121.29	259.87
Air			130	136.36	93.58	749.92	177.59	698.30
TiO_2			59.56	187.64	169.5	235.62	122.6	149.04
Air				181.74	414.79	480.91	273.93	650.99
TiO_2				65.06	208.07	630.17	324.03	156.19
Air					196.16	125.36	231.37	669.27
TiO_2					309.87	544.92	417.35	239.12
Air						428.56	37.48	951.18
TiO_2						131.24	233.66	154.34
Air							203.49	756.69
TiO_2							151.68	396.4
Air								751.85
TiO_2								504.2

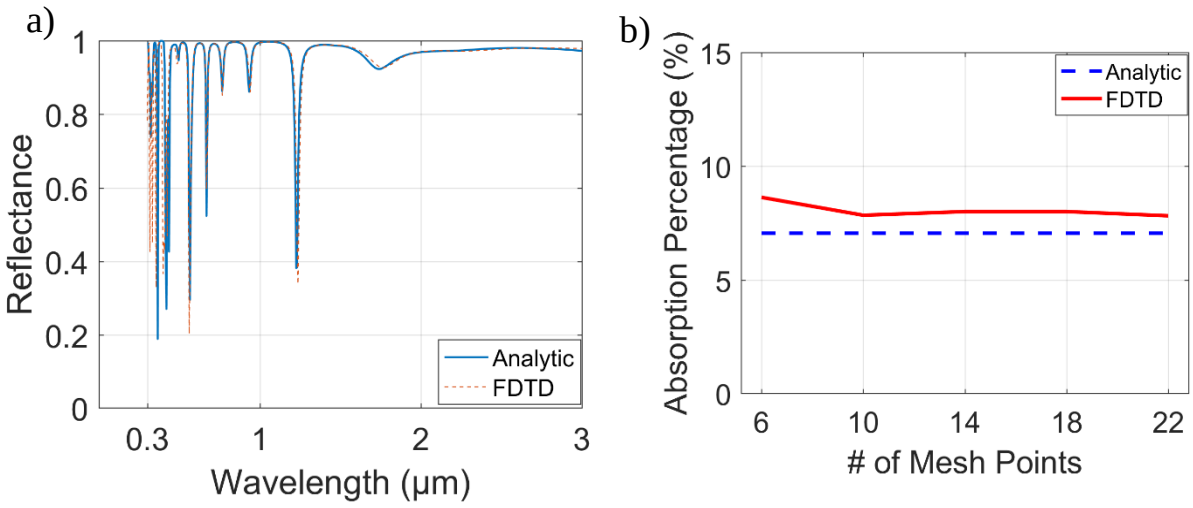

Figure 6. a) Analytical solution of the 8-layered structure obtained analytically by characteristic matrix method [73] vs. FDTD solution with mesh accuracy of 3, which corresponds to mesh points of 14 in Lumerical FDTD. b) Mesh accuracy vs. absorption percentage of the incident radiation.

It is well known that a medium highly reflects incident wave if the optical path at that wavelength is an odd multiple of $\pi/2$. By relying on this, odd multiples of $m\pi/2$ are also marked on the plot depicted in Fig. 5(d). It is observed that there is a perfect fit between $m\pi/2$ and $\delta_{Total,}$ which clarifies the broadband reflectance behavior. Wavelengths of the sharp drops over the spectrum are also marked, which correspond to λ = 0.67, 0.77, 0.93, 1.23, and 1.74 μm wavelengths. Here, sharp dips appear in the regions between the wavelengths where odd multiples are crossing with δ_{Total}.

High reflectance zones over the spectrum are generated when δ_{Total} becomes close to an odd multiple of $\pi/2$, and in between two odd multiples, δ_{Total} approaches to even multiples of $\pi/2$, which is associated with high transmission. Due to the increased number of odd multiple modes at shorter wavelengths, the even multiples and the rate of appearance of sharp dips increase, and more oscillatory reflectance spectrum are observed. As a next step, the effects of lift-off material properties and their dimensions on the reflectance spectrum are studied, and corresponding results are depicted in Fig. 7(a) and 7(b). In Fig. 7(a), n_{Lift} is set to 1.41, and the reflectance spectrum for the updated multi-layer with twelve layers is obtained.

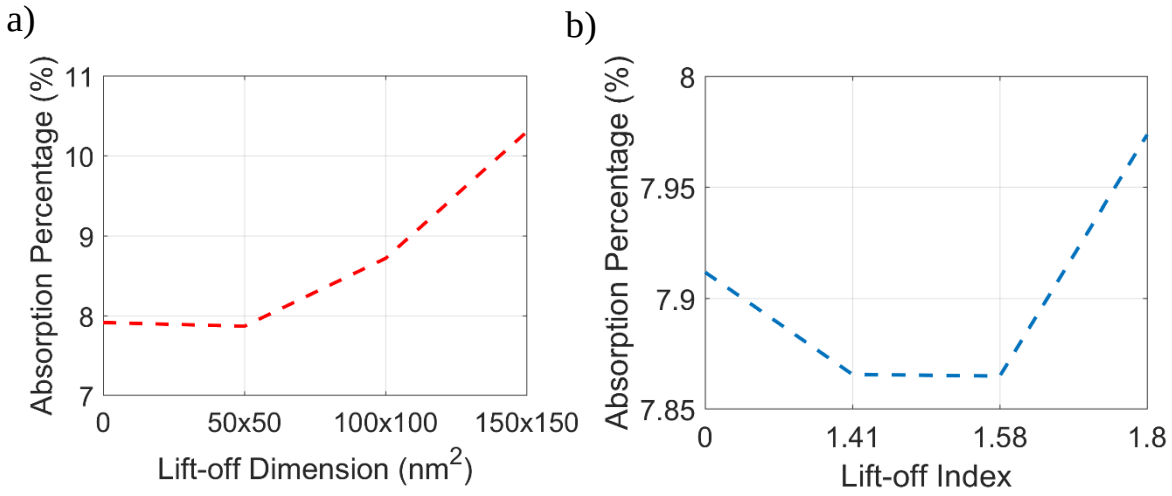

Figure 7. a) Reflectance spectrum of the structure with 8 layers in which lift-off layers (n =1.58) of various sizes are added. b) Reflectance spectrum of the structure with 8 layers in which lift-off layers (100*100 nm) of different refractive indices are added.

A decrease in reflectance, especially at the shorter wavelengths, is observed with increasing lift-off dimensions. This stems from the perturbation introduced in the air medium, which changes the medium's refractive index in the design stage. With increasing volume fraction of the lift-off material, the effective index of the medium starts to deviate more from the presumed value of $n_{Air} = 1$ and alter the interference effects between the mediums. Similarly, in Fig. 7(b), in which the reflectance spectrum for varying n_{Lift} is depicted for 50*50 nm lift-off material dimensions, reflectance intensities start to decrease slightly. Similar reasoning is also valid here.

There are two possible advantages of the inhomogeneous multilayers, in which layers are separated with air gaps, from a thermomechanical point of view. Due to the increased ratio of the refractive indices between the layer materials, higher reflection percentages can be achieved with fewer layers [18]. In addition, air gaps provide space for the layers for thermal expansion under excessive thermal load. In the absence of air gaps, due to the difference between thermal expansion coefficients of the layers, high thermal stresses can occur under excessive thermal load, which leads to mechanical failure of the coating. By introducing air gaps, layers are allowed to expand with less resistance. In addition, separated features are also more advantageous compared to a single large feature. The thermal expansion of a single large feature, in transverse directions, is much larger than the thermal expansion of the smaller features**,** as seen from the mathematical expression for linear expansion under uniform temperature variation $\Delta L = Li * \alpha * \Delta T$ where L_i is the initial length, α is the thermal expansion coefficient, (given as $9.5e10^{-6}$ K^{-1} for TiO_2 [67], ΔT is the temperature change $(T_{Final} - T_{Initial})$, and ΔL is the length change $(L_F - L_i)$. Under constant temperature change over the layer, ΔL can be calculated. In Fig. 8, ΔL is plotted with respect to temperature change, ranging from 100 K to 1000 K, for varying L_i, is demonstrated. As seen, with increasing L_i, ΔL also increases. By introducing inhomogeneities in transverse directions, features will be separated from each other, and they are allowed to expand in those directions, which will be less than the expansion of a single large layer. For this purpose, understanding the effect of periodicity on spectral characteristics is essential.

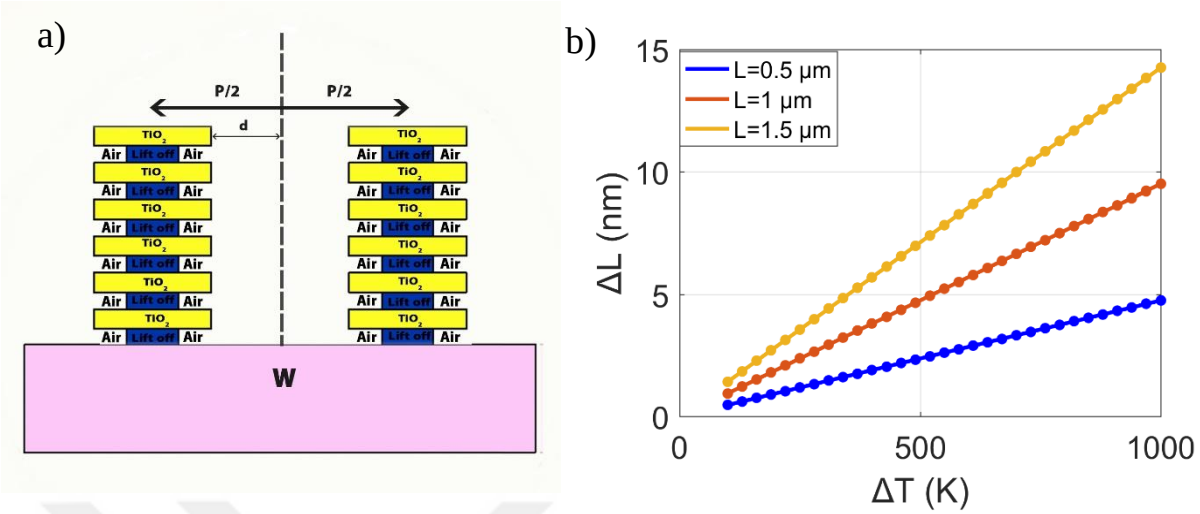

Figure 8. a) Scheme for the periodically arranged Morpho butterfly inspired multilayer features. b) Temperature change vs. linear length change for initial lengths of 0.5, 1 and 1.5 μm.

According to Fig. 3., the distance between two neighboring ridges, (*d*) parameter, is one of the most important variables that affects the structure's reflectivity. In this regard, the average reflectivity for distances of 25, 50, 75, 100 nm has been calculated, and the results can be seen in Fig. 9(a). It can be understood from this figure that increasing the distance between two adjacent ridges decreases the amount of reflectivity from 95% to less than 86%. Furthermore, to compare the effect of the shape of inhomogeneous structures on spectral characteristics, the reflectance of the proposed model for the morpho butterfly wing's nanostructure is depicted in Fig. 9(b-d). Periodicity, *P*, in the calculations is set to 0.5 μm.

According to these results, increasing the gap between two adjacent ridges causes frequent oscillations, especially in shorter wavelengths, which lead to reduced average reflectance. Such oscillations stem from the additional interference effects induced by the air gaps between the periodic structures introduced by non-zero *d*. Contribution from such additional interference effects alters the total optical path that waves travel through the structure. However, the total optical path cannot be calculated by the theory developed for homogeneous layers, which is only applicable for zero *d*. Therefore, a -*S* parameters retrieval method [67] is applied to calculate the -*S* parameters of the studied multi-layer structures. -*S* parameters can be treated as the transfer function of the multi-layer structure, therefore providing an understanding of the optical response of the structures in consideration. Since the reflectance spectrums of the structures are of interest, only S_{11} parameters are analyzed.

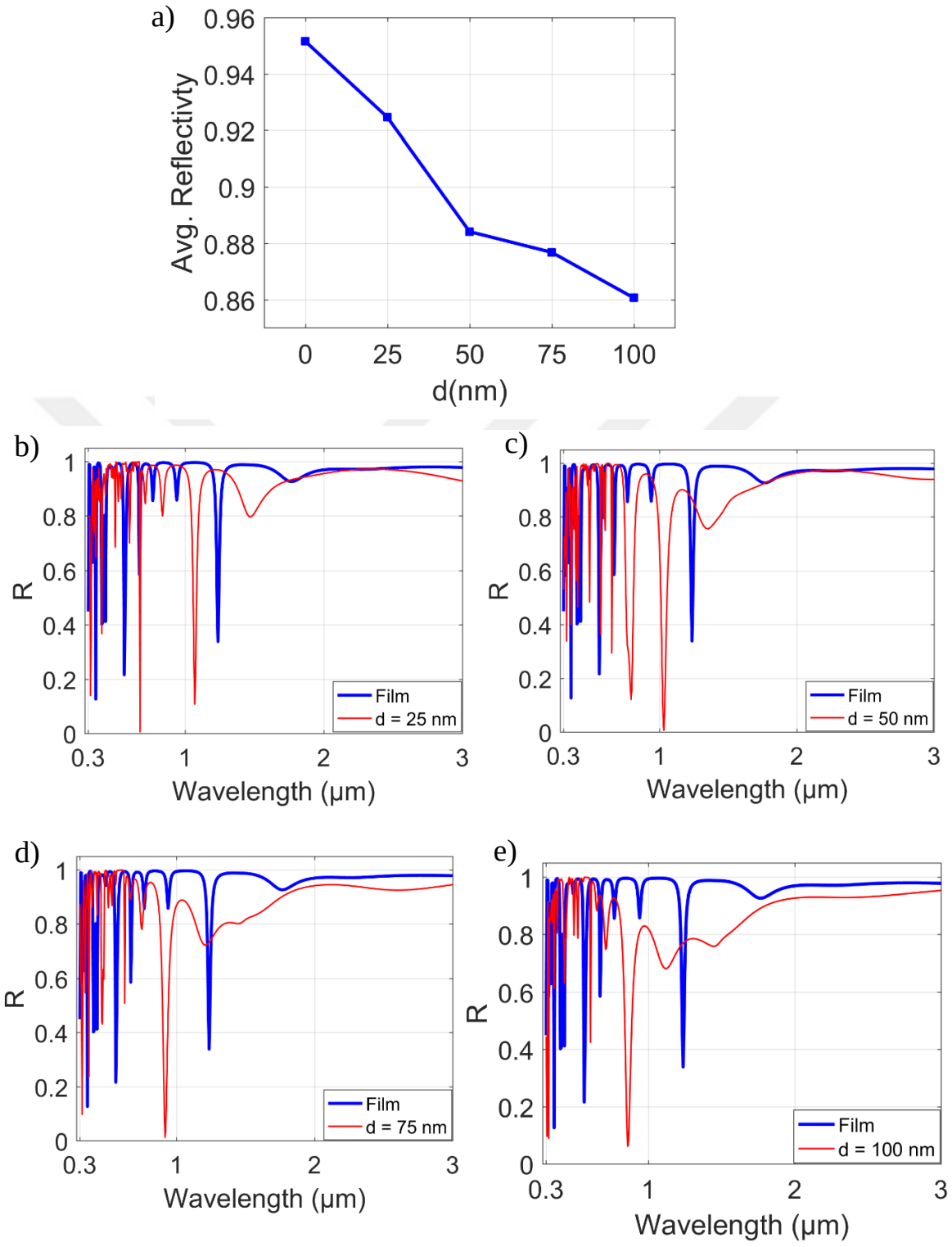

Figure 9. a) Average reflectance of structures for varying distance/periodicity. b-c-d-e) Spectral reflectance of the structures for varying distance/periodicity.

S_{11} parameters are identical to reflectance coefficients given in Eq. (4) and can be represented with magnitude and phase terms. Since phase term determines the optical path that wave travels, phase of S_{11} terms, $<S_{11}$, are studied in the entire spectrum interval. The distinct reflection dips occurring in the 1-1.6 μm spectrum are analyzed to make a detailed evaluation. Then the analysis is extended to a broader spectrum.

In Fig. 10(a), reflectance dips occurring in 1-1.75 μm wavelength interval for the structures with *d = 25, 50, 75,* and *100 nm* are illustrated. As seen, all these dips are shifted to shorter wavelengths compared to homogenous film. A single dip is observed for the structures with *d = 25, 50, 75 nm*, and two dips for *d = 100 nm*. In Fig. 10(b), $<S_{11}$ are plotted concerning wavelength, and even multiples of π are marked with black dashed lines. As seen, the $<S_{11}$ curve of the structure with *d = 25 nm* crosses *0* at 1.45 μm. When considered with the reflectance spectrum depicted in Fig. 10(a), it can be seen that crossing points are very close to reflection dips. Similar trends are observed for the structure with *d =50 nm* whose $<S_{11}$ crosses *0* at 1.3 μm wavelength, which corresponds to the reflectance location dip. Again, single crossing at *0* occurs for the structure with *d =75 nm* and resulting in a single dip in the reflectance spectrum. Finally, the structure with *d = 100 nm* has two crossing points, around 1.18 and 1.57 μm, which result in a distinct and relatively smooth dip in the reflectance spectrum, respectively. To analyze the characteristics at shorter wavelengths that exhibit more frequent oscillations, $<S_{11}$ curves in 0.3 – 3 μm spectrum are plotted with even multiples of π are marked and demonstrated in Fig. 10(c). As seen, the slope of the $<S_{11}$ curves is nearly similar for $\lambda>1$ μm. Therefore, the number of $m\pi/2$ crossings *(m =0,2, 4…N)* are observed in the spectrum is less. With the increasing slope of $<S_{11}$ curves at $\lambda<1$ μm, the number of $m\pi/2$ crossings increases, therefore the number of oscillations increases.

In the light of these results, it is expected that average reflectance will further decrease with increasing *d.* Therefore, to have more efficient thermal management, one should consider the increasing radiative thermal load in the coating with increasing *d* [30,42].

Finally, in addition to the effect of the variation of the refractive index and dimensions of the lift-off materials on the broadband reflectance, the sensitivity of the final structure against possible fabrication imperfections is also studied. For this purpose, ±5 nm was selected, which is within the manufacturing tolerances of the current fabrication technologies, such as electron and ion beam deposition. These modifications are made to the geometric dimensions of the structure with 8

layers which are expressed by 24 geometrical parameters (3 for each layer in 3D) and calculated the reflectance of the structure. Reflection calculations are repeated 10 times. The means and standard deviations for both low and high reflectivity spectrum intervals are plotted in Fig. 11. As seen in Fig. 11, standard deviations are very low (0.2 % and 1 % for $\lambda<1$ μm and $\lambda>1$ μm intervals) with the added possible fabrication errors, which shows the robustness of the structure for possible fabrication errors.

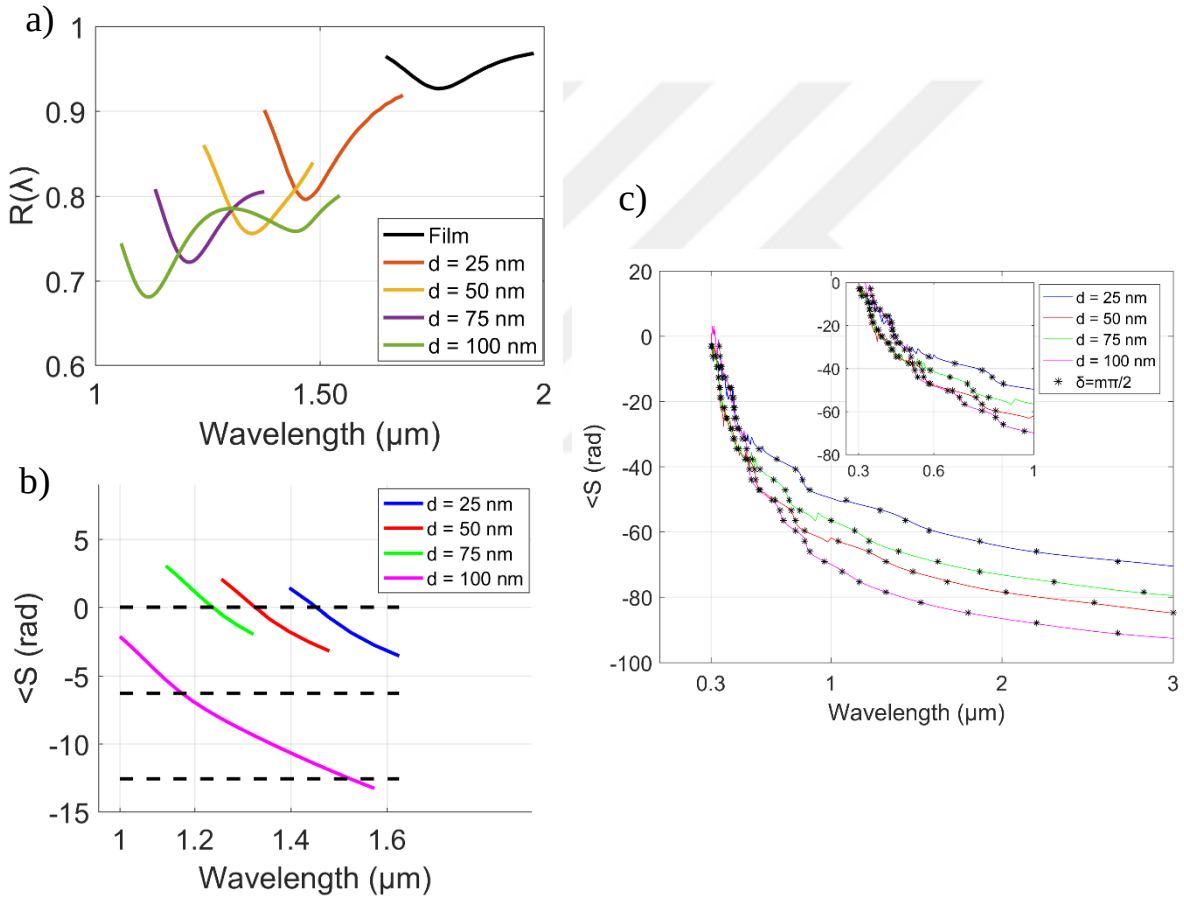

Figure 10. a) Distinct reflectance dips for the structures with different d. b) <S11 curves of the structures with different d for which reflectance dips are shown in Fig. 10(a). c) <S11 curves of the structures with different d in 0.3 – 3 μm intervals with even multiples of $\pi/2$ are marked.

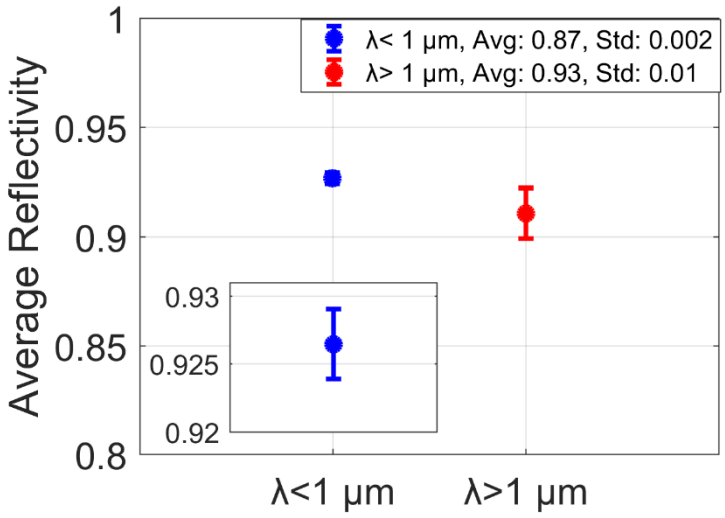

Figure 11. Mean and standard deviations of the average reflectivity of the 8-layered final structure with d = 25 nm both at wavelengths in 0.3 – 1 μm and 1 – 3 μm intervals.

3 BROADBAND REFLECTANCE ENHANCEMENT OF TUNGSTEN WITH ADJOINT-BASED INVERSE DESIGN METHOD

3.1 Problem Definition

Physical properties of materials, along with geometrical aspects, can be defined as the prominent features of designing nano-optical/ nanophotonic structures and devices. In recent decades, many types of research have been done in both areas to increase the optical performance of structures according to their applications, such as reflectivity, absorptivity, or emissivity. The desire to achieve higher reflectivity in the applications such as aerospace applications has led researchers to investigate more in both material and geometrical properties to enhance the optical reflectivity of surfaces.

From a material perspective, utilizing refractory metals like W is one of the most exciting and common methods for higher reflectivity. Despite its high reflection in the wavelength beyond 1.5 μm, high absorptivity in the wavelength below 1.5 μm brings obstacles to structures. Fig. 12 represents the reflection behavior of W in the spectrum of 0.3-1.2 μm. The average reflectivity of W drops to less than 50% in this spectrum. To come up with this problem, one method is employing periodic high index- low index thin film coatings stacked on W, which increases reflectivity up to 90% [18,74]. However, the thermal load and expansion that come from radiation decrease the thermomechanical stability of these structures. One solution to this problem is to manipulate geometry.

From the geometrical aspect, although several researchers have been done to investigate the effect of making holes to achieve higher absorption or emission [78], it has not taken enough attention to enhance reflectivity. To explore the impact of creating holes on the reflectivity of Tungsten, periodic holes with the size of 50*50 nm^2 drilled into it, and the results compared with the base substrate without holes in Fig. 12. The average reflectance of both models shows that making these holes increases absorptivity. As described previously, coating Tungsten substrates with high index/low index thin films significantly impact enhancing reflectivity. The primary goal of this chapter is to determine whether making holes can boost reflectivity using these coatings.

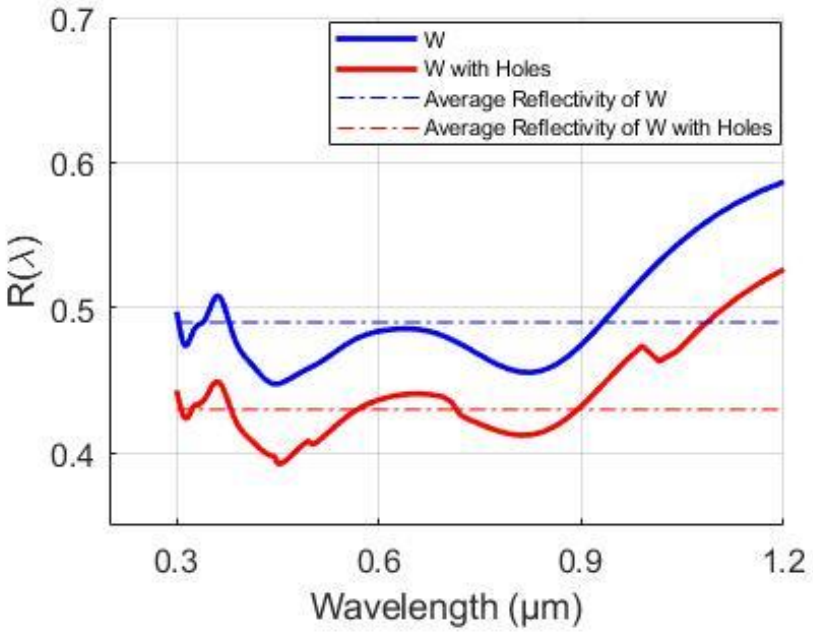

Figure 12. The comparison of reflectivity of Tungsten with and without periodic holes, dashed lines: average reflectivity of both models

3.2 Methodology

Maxwell's equations were the foundation for forecasting that light is an electromagnetic phenomenon once they were developed, and they have subsequently enabled every photonic technology. Accordingly, solving Maxwell's equations with robust and quick methods is the issue for many studies in this area. Various strategies have evolved as feasible methodologies, ranging from finite-difference time-domain (FDTD) to boundary element method (BEM). They're all designed to indicate the results of fields and/or eigen-frequencies for a particular geometry. This type of problem is called the forward problem. On the contrary, inverse problem, which means the geometry required for a desired electromagnetic response, is more beneficial. Answering this question forges a new route in computational electromagnetics by moving away from the forward problem.

The forward problem is more accessible than the inverse one. Physical reality mandates that there be only one solution for the forward issue with a given shape and collection of sources.

However, specifying a collection of attributes does not guarantee that geometry will exist or, if it does, that it will be unique. People often try a slightly modified version of the inverse problem by answering what shape gets the required electromagnetic response the closest to get around these problems. In this perspective, inverse design difficulties are transformed into optimization problems, with the intended functionality constrained by the requirement that all fields and frequencies be Maxwell's equations solutions. The general electromagnetic inverse design issue can be expressed mathematically as follows:

$$\begin{aligned} &\underset{\bar{\bar{\epsilon}},\bar{\bar{\mu}}}{Optimize} \quad F(E,H) \\ &subject\ to \quad \nabla.\bar{\bar{\epsilon}}E = \rho \\ &\qquad\qquad \nabla.\bar{\bar{\mu}}H = 0 \\ &\qquad\qquad \nabla \times E = -j\omega\bar{\bar{\mu}}H \\ &\qquad\qquad \nabla \times H = J + j\omega\bar{\bar{\epsilon}}E \end{aligned} \tag{1}$$

According to the four Maxwell partial differential equations, the goal is to identify the permittivity and the permeability tensor that optimize the function F (E, H). PDE-constrained optimization is the name given to this method of inverse design. The photonic inverse design issue can be approached in a variety of ways. The efficiency of any technique in arriving at a design is the yardstick by which it is judged. The solution of the forward problem, which is often repeated for many distinct designs, is the most time-consuming component of the inverse design for photonic design challenges. As a result, the number of simulations required by a method is a reliable indicator of its efficiency. Although some methods like the Genetic algorithm optimize the two-dimensional problems and computationally modest three-dimensional problems, because the method often necessitates tens of thousands of simulations, it is impractical for three-dimensional optimizations with a large parameter space.

On the other hand, topology calculus provides a foundation for effective optimization with many fewer simulations. Topology calculus is the infinite-dimensional space of shape and topology's parallel to the conventional differential calculus of finite-dimensional spaces. It turns out that computing the derivative of an objective function regarding the entire infinite-dimensional space requires just two simulations; moreover, converging to an optimal design often requires

fewer than a hundred iterations. When compared to other approaches, shape calculus frequently allows for a 100- or 1000-fold reduction in the number of simulations necessary.

3.2.1 Inverse Design Calculations for a Photonic Problem

Most of the optimization strategies are gradient-based. These are frequently iterative algorithms that require derivative information at each iteration. The adjoint technique, also known as the reverse approach, calculates gradients by adding new variables to the equation. One may skip doing certain sections of the gradient computation by allowing these variables to meet a particular condition known as the adjoint equations. In other words, it pays the price for solving adjoint equations and gaining something by canceling out other calculations. The adjoint or reverse technique should be implemented when it is required to compute the sensitivities of a scalar or low-dimensional function regarding many factors. Forward sensitivity analysis is arguably more suited when it is necessary to compute sensitivities from a few parameters to a high dimensional function.

Compared to heuristic techniques, gradient calculation in topology optimization would enhance convergence to a geometry that demonstrates a local minimum for the given objective function [75]. However, for vast design spaces, such as N simulations with FDTD technique for gradient calculation for a structure with N design parameters [76], the calculation of the gradient itself might be computationally intensive. The adjoint approach has been used [76,77] for the gradient calculation to prevent such computational load. The gradient is determined using the methods described in [76], which discusses how any disturbance on the surfaces may be considered a dipole scatterer and how this can quantify the influence of such perturbations on the figure of merit, such as reflection. The gradient information is then utilized to change the structure's topology. Finally, the reflection for the new design is calculated using the conservation of energy and the fact that the structure is opaque. The chosen approach allows gradient computation for each geometry with two simulations, front and backward (adjoint). The gradient is generated in a computationally efficient manner using this technique, and it has been used to alter the surface geometry of the starting structures.

The gradient computation is critical here, as it necessitates both a mathematical and physical grasp of Maxwell's equations to describe the issue adequately and execute the solution. As a result, the mathematical formulation of the gradient calculation issue for a figure of merit that is reliant

on *E* and *H* fields is summarized, and the physical understanding necessary to apply the suggested solution is given. FDTD [68] solves the required equations for the gradient computation, and the simulation physics is also presented.

For a particular figure of merit function, F, the electric, *E*, and magnetic, *H*, components are as follows:

$$F(E,H) = \int_S f\big(E(x),H(x)\big)d^2x \tag{2}$$

F is the objective function that is used to optimize a function, *f*, which is made up of *E* and *H* fields across a surface, *S*, describes the change in the objective function of this type as follows [76]:

$$\Delta F = 2Re\int_{S'} d^2x' P_j^{ind}(x')\int_S d^2x\left[G_{ji}^{EP}(x',x)\frac{\partial f}{\partial E_i}(x) - G_{ji}^{EM}(x',x)\frac{1}{\mu_0}\frac{\partial f}{\partial H_i}(x)\right] \tag{3}$$

The necessary mathematical methods to go from Eq. (2) to Eq. (3) are detailed in [76]. The following is the physical interpretation of Eq. (3):

Induced polarization intensity, P^{ind}, owing to *E* fields from electric and magnetic dipoles with amplitudes of $\partial f/\partial E$ and $(\mu_0)^{-1}\,\partial f/\partial H$ is quantified. More intuitively, any geometrical disturbance on the design surface, *S'*, is treated as a dipole scatterer, and the reciprocity of Maxwell Green's functions is relied upon.

$$G_{ij}^{EP}(x,x') = G_{ij}^{EP}(x',x) \tag{4}$$

$$G_{ij}^{HP}(x,x') = -G_{ji}^{EM}(x',x) \tag{5}$$

E and *H* fields produced by electric and magnetic dipoles put over the *S* may be calculated to predict changes in *E* fields induced by geometrical perturbations with the volume of V and permittivity of on *S'*.

For the reflection optimization, F is defined as,

$$\mathrm{F(E,H)} = \frac{\frac{1}{2}\int_S Re\left(\overrightarrow{E^R}(\lambda)\times\overrightarrow{H^R}(\lambda)^*\right)dx}{I(\lambda)} \tag{6}$$

I is the incident power intensity, while E^R and H^R are the reflected electric and magnetic fields. Calculating $\partial f/\partial E$ and $(\mu_0)^{-1}\,\partial f/\partial H$ yields the dipole sources' amplitudes, which are calculated in [78].

Following the calculation of these amplitudes, the second integral in Eq. (3), referred to as $E^A(x')$ (adjoint fields) in [76], is realized in FDTD using electric and magnetic dipoles dispersed

throughout the measurement plane. The derivative regarding permittivity is derived by putting $P^{ind}=\Delta V\Delta\varepsilon E^{Old}(x')$ in Eq. (3).

$$\frac{\partial F(\lambda)}{\partial \varepsilon(\lambda)} = 2Re \int_{S'} \Delta V E_j^{Old}(x').E_j^{A}(x')d^2x' \tag{7}$$

The fields from old (ahead) and adjoint (backward) simulations are used to determine the change of F with respect to ε for a known perturbation volume, as shown in Eq. (7). The influence of various geometrical perturbations in the design space on F is estimated in this manner, and final structures are produced repeatedly, in a computationally efficient way, by computing the gradient with two simulations each iteration. Fig. 13 is an excellent visualization brief of what is explained in this section.

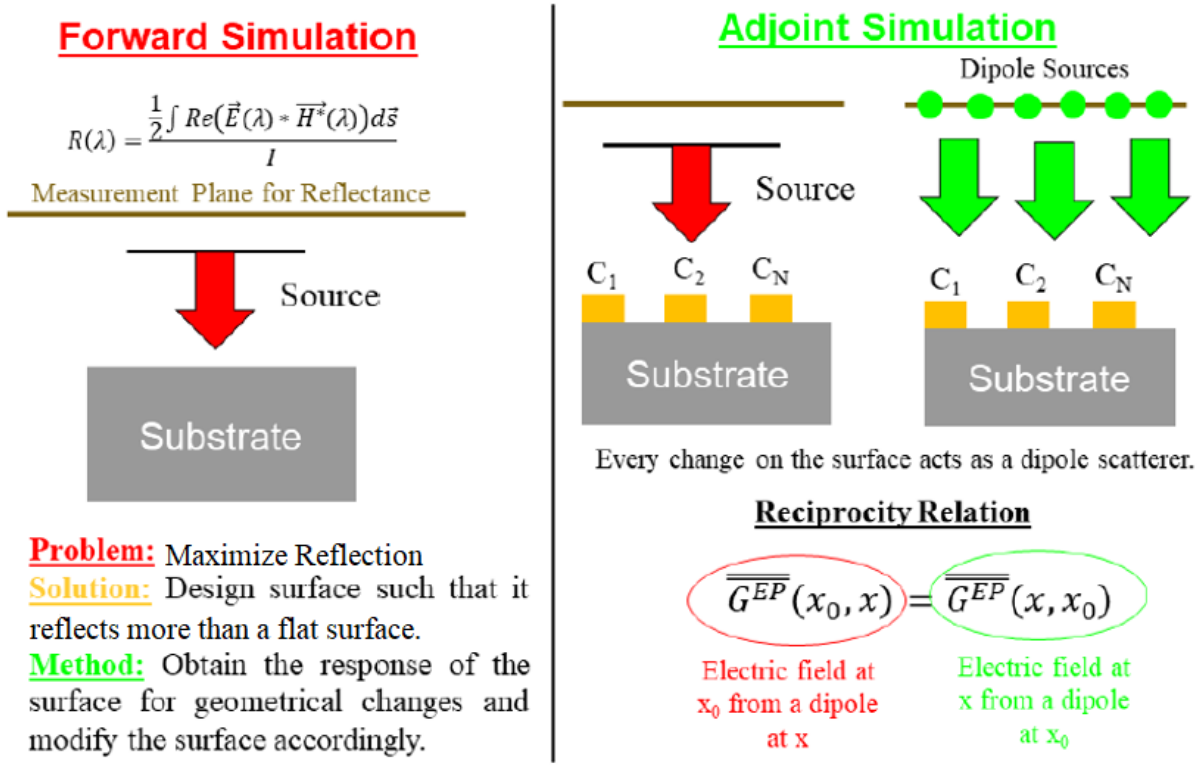

Figure 13. A brief visualization of forward and adjoint calculations

The numerical implementation of the inverse design approach discussed in this chapter is schematically illustrated in Fig. 14. MATLAB is used to do the overarching inverse design, linked to full-wave electromagnetics solvers like Lumerical FDTD Solutions. The geometry is stored in a MATLAB data structure, then sent to the electromagnetic solver through solver-specific code. The solver runs both simulations and outputs all the field data. The procedure iterates once the

shape derivatives and updates are completed in MATLAB. Several geometric representations can be used. Level set functions exist for a generic class of smooth forms, such as ellipses, rectangles, and other elementary structures, which might also be utilized to construct more complicated geometries.

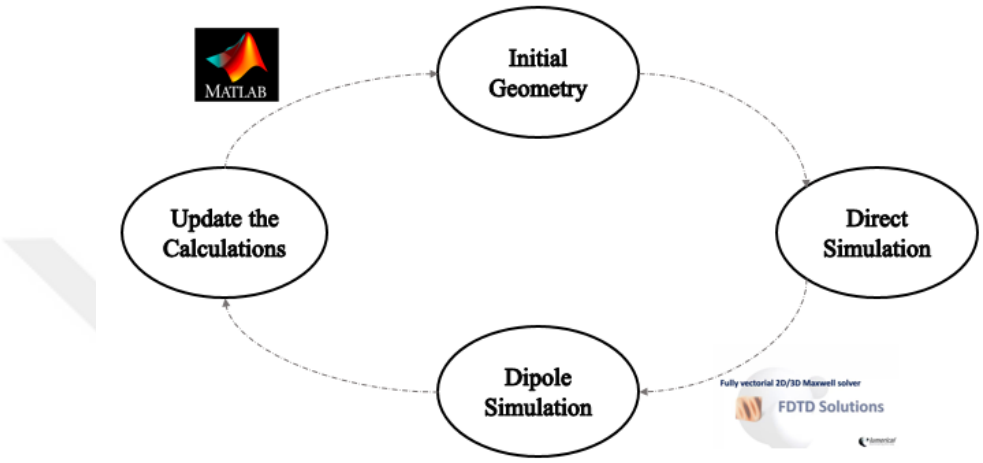

Figure 14. A numerical implementation of the inverse design approach [76]

3.2.2 The proposed Initial Design for the Inverse Design Approach

As mentioned earlier, initial geometry is unknown in the inverse design method. Therefore, it is preferable that a primary proposed model can satisfy the essential feature of the required objective function, which is the reflection in the current work. To satisfy this condition, one method is to utilize the impedance mismatch method introduced in chapter two, where the optimized layers of low index/high index materials (SiO_2/TiO_2) stacked on Tungsten substrate gives higher reflectivity and shows to be effective as an initial model here. Besides, the effect of periodic holes drilled in thin films is investigated to clarify the impact of periodicity on the reflectivity of the multilayer coatings and determine whether it is possible to use these structures as our initial structures. In this regard, a proposed initial design model can be selected after analyzing the multilayer coating with and without periodic holes. A schematic model of the proposed structure is shown in Fig. 15, in which *l* represent the size of holes.

To improve this initial design, which is obtained by intuition and parametric analysis, topology optimization is adapted, which allows exploring non-intuitive possibilities which exhibit higher reflection.

Lumerical FDTD solver is used to simulate the models obtained from impedance mismatch code and link to MATLAB to calculate the inverse design and adjoint calculations. Therefore, the periodic boundary condition is applied on the x-y plane, where the PML boundary condition is used in the z-direction. A linearly polarized plane wave traveling in the z-direction is used to stimulate structures. The required *E* and *H* fields are derived from the simulation setup mentioned above. The mathematical procedure mentioned in the previous section is used to determine the gradient with respect to F, which is reflectivity (R). In the adjoint simulation, as shown in Fig. 13, a plane wave source is replaced by numerous dipoles, the amplitudes of which are determined according to [78]. The simulations are run in the spectrums with the wavelength with the highest reflection chosen, and the shape is adjusted based on the gradient at that wavelength to minimize absorption and maximize reflection.

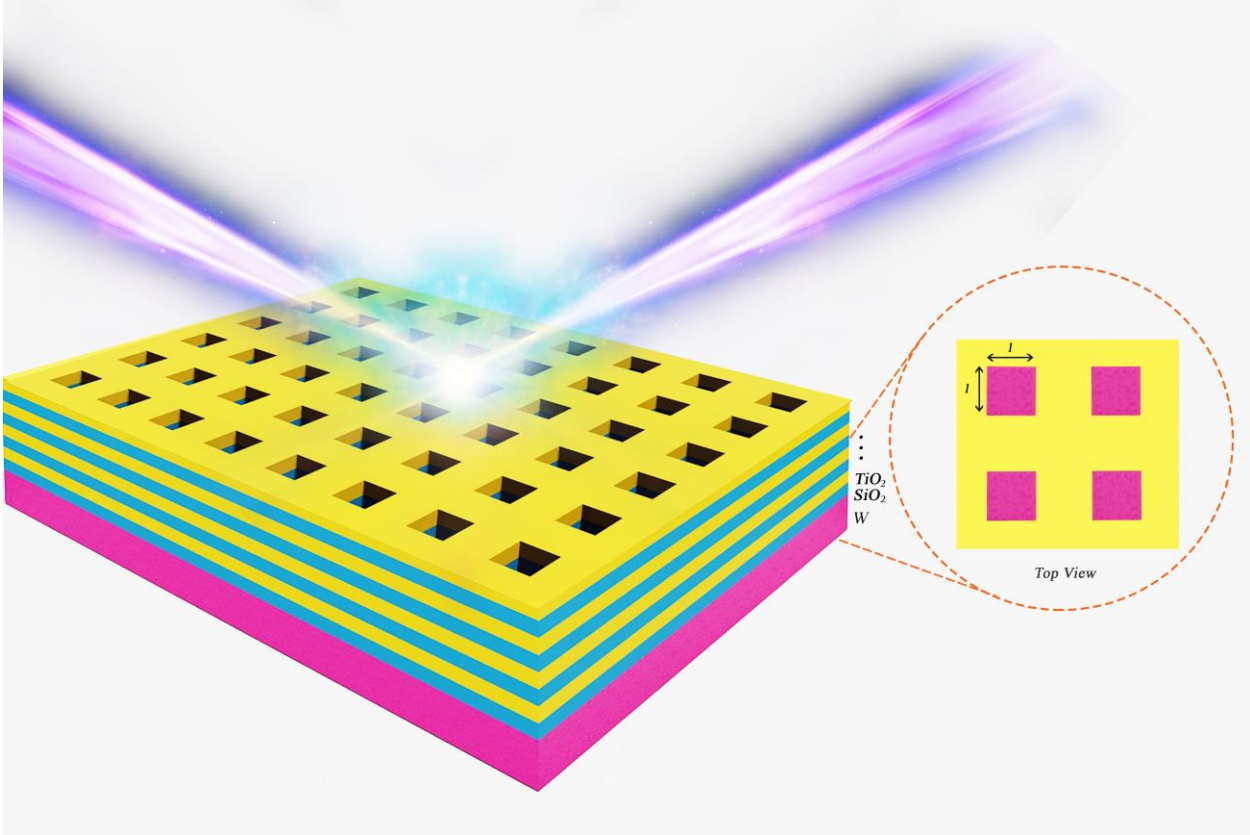

Figure 15. Schematic representation of initial design model

3.3 Results and Discussions

As mentioned in the preceding section, the first goal of the current study is to boost Tungsten's reflectivity by utilizing SiO2-TiO2 multilayer coatings to introduce an initial geometry for the inverse design calculations. The influence of increasing the optimal layers on the average reflectivity of Tungsten is shown in Fig. 16(a), and the associated materials and thicknesses are listed in Table 2. The figure is separated into wavelengths less than 1.2 μm, where the average reflectivity of W substrate is around 50%, and wavelengths higher than 1.2 μm that the average reflectivity of W substrate is about 80%, as shown by dashed lines. The reflectivity of both spectrums riches to nearly 95% by increasing the number of the optimal thin film layers to sixteen. According to the impedance-mismatch analysis, it is concluded that if the optical path is an odd multiple of π/2, the medium substantially reflects the incident wave. Furthermore, the even multiples of π/2, between two odd multiples, are associated with strong transmission [74]. Therefore, the even multiples and the rate of occurrence of sharp dips rise as the number of odd multiple modes increases.

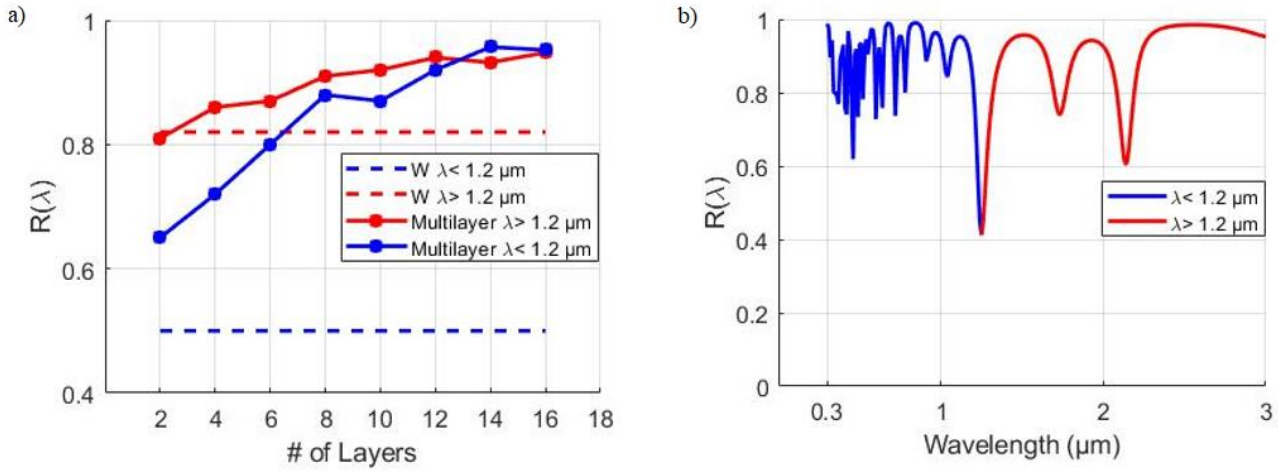

Figure 16. a) The effect of increasing the number of layers on reflectivity, b) The reflectance of Tungsten coated by twelve layers of SiO_2/TiO_2 in 0.3-3 μm with α=.7

Table 2. Thicknesses of the layers used in the SiO_2/TiO_2 multilayers with layer numbers of 2, 4, 6, 8, 10, 12, 14, and 16 on top of 500 nm W.

Layer Material	# of Layers							
	2	4	6	8	10	12	14	16
W (500 nm)	Thickness [nm]							
SiO_2	76.99	173.42	193.31	76.50	84.18	332.69	90.33	59.1
TiO_2	231.14	240.24	82.02	288.96	136.67	76.70	278.34	107.56
SiO_2		89.1	163	154.48	81.58	123.93	85.64	360.62
TiO_2		58.14	60.57	65.69	69.34	193.28	53.31	272.68
SiO_2			92.33	103.21	166.53	499.99	142.78	256.79
TiO_2			52.57	33.44	46.66	54.92	77.09	64.98
SiO_2				232.94	354.18	159.26	183.15	246.45
TiO_2				76.68	185.87	103.50	251.82	117.80
SiO_2					401.25	171.79	106.13	416.61
TiO_2					410.08	127.62	479.76	86.96
SiO_2						85.14	92.89	496.48
TiO_2						53.77	451.84	144
SiO_2							176.70	104.95
TiO_2							176.87	265.99
SiO_2								273.56
TiO_2								77.25

The reflectivity of coated Tungsten with twelve numbers of thin-film SiO2/TiO2 layers is depicted in Fig. 13(b). There are three dips in the wavelengths of 1.25,1.8, and 2.2 μm, and the oscillations at shorter wavelengths come from the even multiples of π/2, which can be validated by the concept of impedance mismatch method introduced in the previous chapter [74].

As discussed earlier, inhomogeneous multilayers, in which air gaps separate layers, have benefits over homogeneous multilayers. Higher reflection percentages can be attained with fewer layers due to an improved ratio of refractive indices between the layer materials [18]. According to this point, first, the effect of periodic holes is investigated to find out the impact of the size of holes on reflectivity. Using the results obtained from the simulations guide to an effective geometry to start the inverse design calculations.

The main concern here is how holes affect reflectivity and whether it is possible to increase reflectivity by altering the holes. To answer this question, the average reflectivity for the holes with l = 25, 50, 75, and 100 nm has been analyzed for the coated Tungsten with twelve thin films of SiO_2/TiO_2 stacked on it, and the findings are compared with the homogeneous structure as shown in Fig. 17. According to Fig. 17(a), although reflectivity drops with increasing the size of holes, the reduction exceeds no more than 5% when l increases to 50nm. Significantly, the reflection drops less than 1% for the holes with l = 25nm, which can be an excellent choice to start the shape optimization calculations.

Another finding concluded from these simulations is shown in Fig. 17(b-d), where widening the space between two neighboring holes creates more oscillations at shorter wavelengths, resulting in lower average reflectance. The additional interference effects caused by the air gaps between the periodic structures introduced by non-zero l cause such oscillations. Contributions from such extra interference effects alter the overall optical path that waves travel through the structure. However, decreasing the volume fraction of the layers with the air gaps reduces the medium's refractive index, which leads to higher reflectivity. Furthermore, increasing the size of periodic holes shifts the dip points to shorter wavelengths. For instance, the deepest point moves from 1.25 μm in the hole size of 25 nm to 1.1 μm for l = 10 nm. A better understanding of the relying physics behind this behavior can be helpful in the adverse design calculations. In this regard, -S parameter calculations are done similar to what was done in the previous chapter.

The $<S_{11}$ parameter is used because just the reflectance spectrums of the structures are of importance. The reflection dips occurring between 1–1.6 μm for different models are studied to make a complete assessment. The analysis can then be expanded to include a broader range of variables. Reflectance dips in the 1–1.6 μm wavelength region for structures with l = 25, 50, 75, and 100 nm are shown in Fig. 18 (a).

$<S_{11}$ is displayed in terms of wavelength in Fig. 18(b), and even multiples of π are highlighted with black dashed lines. The $<S_{11}$ curve of the structure with l = 25 nm crosses 0 at 1.25 μm, as can be shown. Compared to the reflectance spectrum shown in Fig. 18(a), crossing points appear close to reflection dips. The structure with l =50 nm, whose $<S_{11}$ crosses 0 at 1.23 μm wavelength, corresponds to the reflectance location drop, shows similar tendencies. For the structure with l =75 nm, a single crossover at 0 occurs, resulting in a single dip in the reflectance spectrum. Finally, the structure with l =100 nm has two crossing points, at 1.1 and 1.5 μm, resulting in a prominent and reasonably smooth drop in the reflectance spectrum.

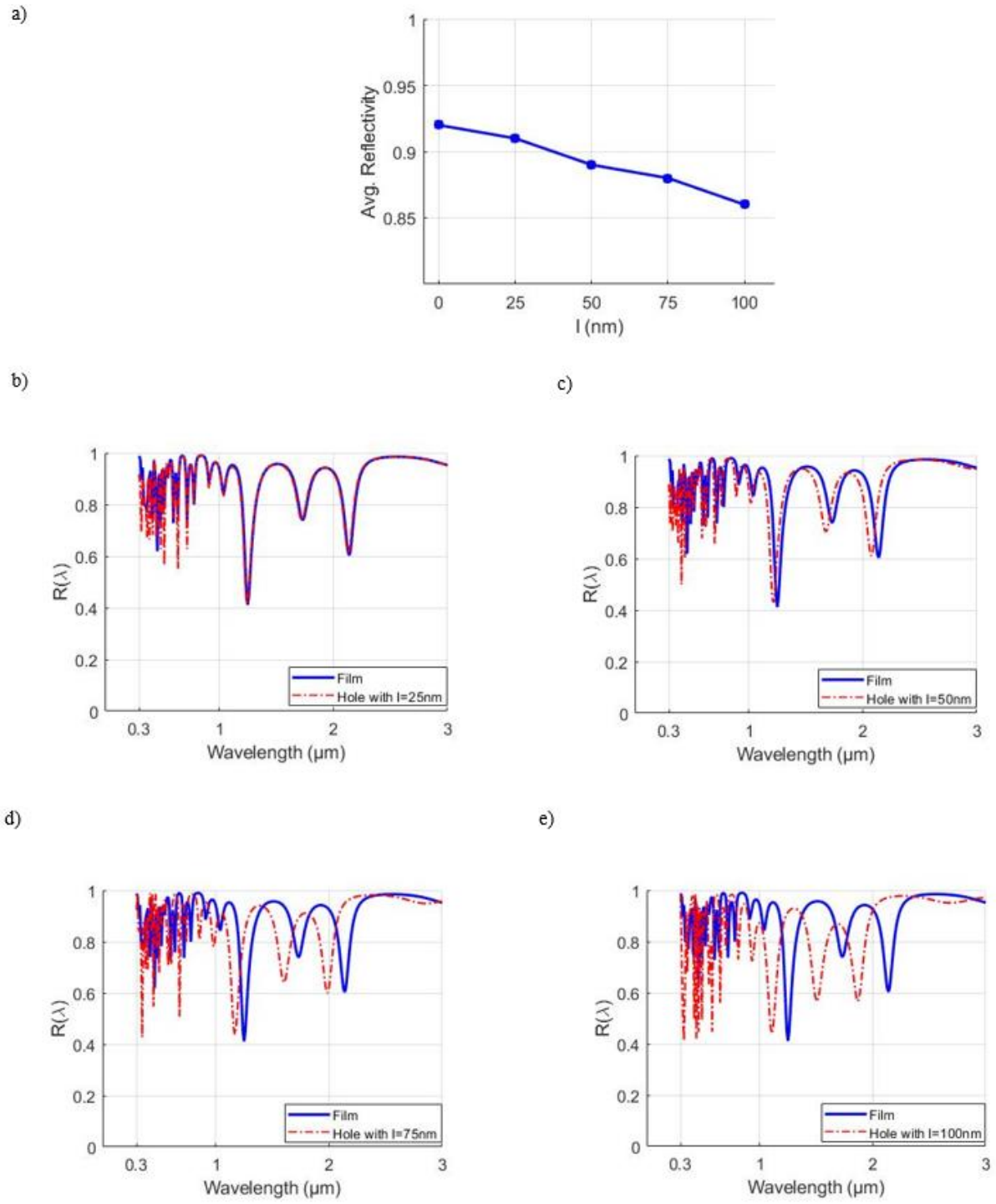

Figure 17. a) Average reflectance of structures for various hole sizes (*l*). b-c-d-e) Spectral reflectance of the structures with different *l* dimensions.

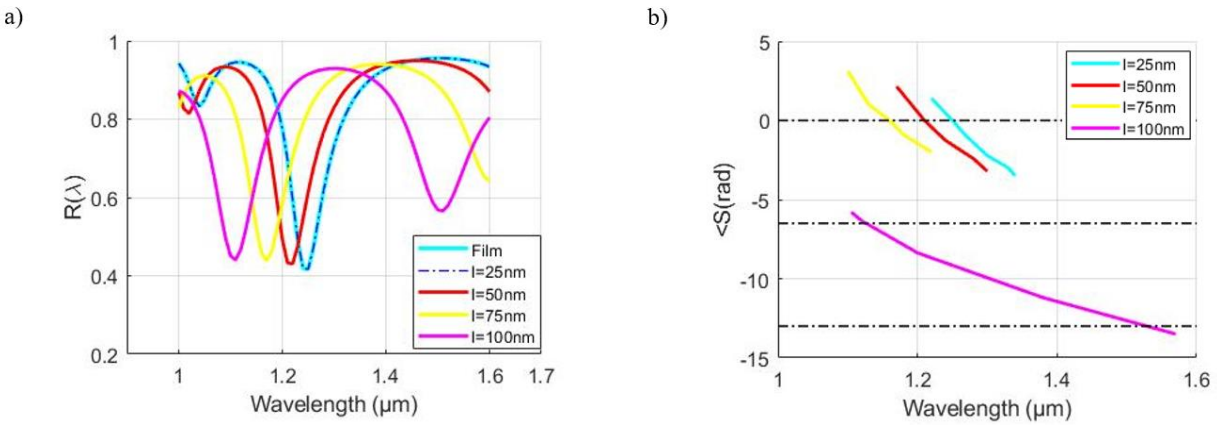

Figure 18. a) The reflectance dips for the structures with different *l* size between 1-1.6 μm. b) <S11 curves of the structures with different *l* for which reflectance dips are shown in Fig 18(a).

After analyzing the dip points for the structure with twelve optimized layers for different hole sizes, the one with *l* =25nm is selected as the initial geometry to import to the inverse design calculations. As discussed, the deepest point occurs at 1.25 μm and shifts with increasing the dimension of the hole. Therefore, because of the massive amount of required calculation time, the narrowband wavelengths of 1-1.6 μm are selected to analyze.

Following the steps discussed in section 3.2.1, the gradient is calculated using the adjoint method iteratively to enhance the reflectivity of the initial structure. Fig. 19 shows the final geometry for the selected initial model after shape calculations. The calculations are converged after 200 iterations to obtain the current geometry. As seen in Fig. 19, some discontinuities appear because the algorithm adds material to the pixel with the highest sensitivity to change. Fig. 20 shows the reflection throughout the selected spectrum for the resulted structure. As shown in this figure, the used approach improves the reflectivity of selected spectra compared to the initial constructions. With this topology optimization approach, the deepest point at 1.25 m, with a reflectivity of 42%, riches to reflectivity around 50%. The average reflectivity in this narrow band spectrum increases approximately up to 3%, which is acceptable and demonstrates the implemented approach's robustness and effectiveness in the reflection problem.

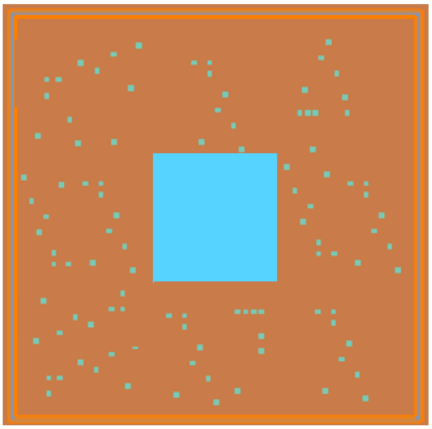

Figure 19. The obtained topology with inverse design approach for twelve optimized number of SiO_2/TiO_2 with a hole with l =25 nm

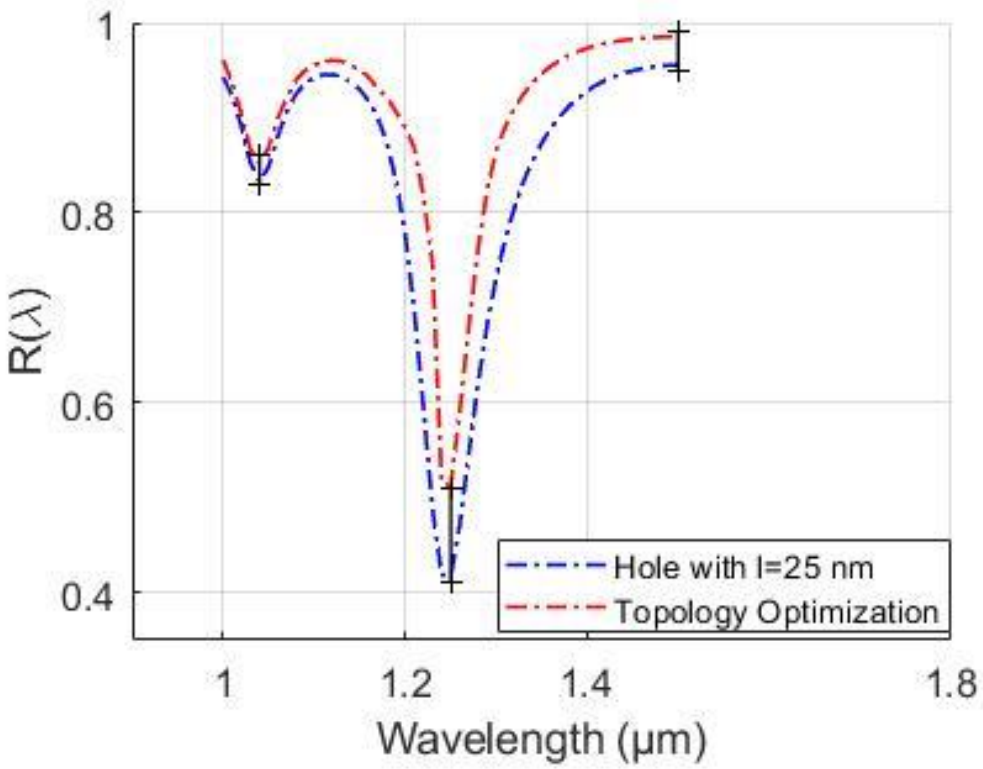

Figure 20. The comparison of reflectivity for the twelve number of SiO_2/TiO_2 multilayer structures with l =25 nm, with and without implementing inverse design method in the wavelengths of 1-1.6 μm.

According to the results, the two most challenging problems still require further work. As previously noted, the computations take a long time to complete. After pursuing the adjoint computation steps, a plane wave source is replaced by numerous dipoles. The Lumerical FDTD solver performs this phase, which requires extensive time to simulate the *E* and *H* fields. This is the primary reason why a narrow band spectrum was investigated in the current section.

Also, the fabrication of the obtained structure is the other essential consideration. Fabricating a geometry with holes about 2 nm is extremely difficult. To tackle this problem, one option is to use the Effective Medium Theory (EMT). This method is an analytical or theoretical model representing the macroscopic characteristic of composite materials is referred to as effective medium approximations or effective medium theory. EMTs are developed by averaging the multiple values of the constituents that directly make up the composite material. Although, in general, the constituent level values are inhomogeneous, and the exact calculation of these amounts is somehow incredibly impossible, EMT demonstrates to have acceptable approximations to describe proper parameters, including the effective permittivity and permeability of the materials as a whole. Effective medium approximations, in this sense, are descriptions of a medium (composite material) obtained from computations based on the attributes and relative percentages of its constituents [79,80]. According to these points, this method can offer two benefits for the current work: the equivalent used materials with no holes obtained from this approximation, leading to make the structure more accessible. In addition, the oscillations caused by air gaps will reduce, resulting in increased reflection.

4 CONCLUSION

In summary, in the first part of the thesis, optimized multi-layer coatings inspired from morpho butterfly structures are proposed to increase the reflectivity of Tungsten in the broadband spectrum of 0.3-3μm. The impedance mismatch method results indicate that stacking eight number of TiO_2-Air (As high index-low index) layers on the tungsten substrate with the optimized thicknesses increases the average reflectivity of Tungsten up to 95% in the broadband spectrum. It is shown that lift-off dimensions and optical properties do not significantly impact the selected values. While the inhomogeneities in the transverse direction do not cause a significant reduction in the reflectance, a slight decrease in magnitudes is observed due to an increased number of sharp reflection dips over the spectrum. Calculated -S parameters of the final inhomogeneous structures show that reflection dips occur when <S becomes multiples of π, and the number of crossings increases at shorter wavelengths. Spectral analysis of different distances between the ridges, *d*, indicates that reflectance of the coating is reduced with increasing *d*. The highest reduction rate is observed for *d~100 nm*, for which average reflectance drops to 86 % levels at most. The robustness of the final structure against possible fabrication imperfections described by adding ±5 nm tolerance in dimensions indicates the means of the average reflectance changes by % 1 at most at longer wavelengths.

The second part introduces optimized multi-layer coatings achieved by the shape calculations. To select a proper initial geometry, which plays a starter role in the inverse design calculations, a twelve optimized number of SiO_2/TiO_2 thin film layers stacked on Tungsten substrate obtained from impedance mismatch method analysis discussed in the previous part. Regarding the benefits of air gaps, the effect of making periodic holes of various sizes is explored. The same amount of reflection resulting from the hole with l =25nm indicated that this structure could be substituted with the previous design without holes. The average reflectivity of up to 90% is achieved for the initially proposed geometry. To have a comprehensive attitude toward the inverse design approach and employ it for the initial model, the origin of the dip points and the effect of the size of holes investigated using -*S* parameter calculations. According to the findings, the dip points are analyzed, and then, the narrowband spectrum of 1-1.6 μm is selected to be calculated with the adjoint method. The reason to choose narrowband spectra is the issue with the tremendous amount of required time to solve the problem, which is one of the ongoing works of this project.

After implementing the inverse design method, the average reflectivity increased more than 3% at 1-1.6 μm, which indicated the effectiveness of the employed method in the current problem. The challenging concerns for the fabrication of obtained structures are recognized, and possible solutions are introduced.

5 FUTURE WORKS

The following headlines are proposed for furthering the work based on the research output of this thesis:

- The most apparent characteristic of the Morpho butterfly wing's nanostructure is its beautiful colors, along with its thermomechanical advantages. Therefore, the proposed structure can be utilized in color-based radiative cooling problems. Besides, both spectral and radiative aspects of the problem can be evaluated, and more elaborate analysis can be undertaken by integrating spectral design methodologies with commercial heat transfer solutions such as COMSOL Multiphysics. The influence of layer materials and thicknesses on the thermal component of the issue owing to conduction between layers and convection with the environment may be examined using this technique.
- For the second part of the thesis, the mentioned concerns include implementing the calculations to a broadband spectrum by reducing the calculation time and solving the fabrication issue by utilizing the Effective Medium Theory can be a subject to work more. Besides, the adjoint-based topology optimization approach could be used for a wide range of reflection control challenges to improve the desired spectrum performance. It will make it easier to explore non-intuitive topologies while also enhancing performance.

REFERENCES

1. S. Y. Jeong, C. Y. Tso, J. Ha, Y. M. Wong, C. Y.H. Chao, B. Huang, and H. Qiu, "Field investigation of a photonic multi-layered TiO2 passive radiative cooler in sub-tropical climate," Renewable Energy 146, 44–55 (2020).

2. M. A. Kecebas, M. P. Menguc, A. Kosar, and K. Sendur, "Spectrally selective filter design for passive radiative cooling," J. Opt. Soc. Am. B 37, 1173 (2020).

3. H. Ma, K. Yao, S. Dou, M. Xiao, M. Dai, L. Wang, H. Zhao, J. Zhao, Y. Li, and Y. Zhan, "Multilayered SiO2/Si3N4 photonic emitter to achieve high-performance all-day radiative cooling," Solar Energy Materials and Solar Cells 212, 110584 (2020).

4. Yalçın, R. A., Blandre, E., Joulain, K., & Drévillon, J. "Daytime radiative cooling with silica fiber network," Solar Energy Materials and Solar Cells 206, 110320 (2020).

5. A. Kong, B. Cai, P. Shi, and X.-C. Yuan, "Ultra-broadband all-dielectric metamaterial thermal emitter for passive radiative cooling," Optics Express 27, 30102–30115 (2019).

6. Hervé, A., Drévillon, J., Ezzahri, Y., & Joulain, K. "Radiative cooling by tailoring surfaces with microstructures: Association of a grating and a multi-layer structure," Journal of Quantitative Spectroscopy and Radiative Transfer 221, 155-163 (2018).

7. M. A. Kecebas, M. P. Menguc, A. Kosar, and K. Sendur, "Passive radiative cooling design with broadband optical thin-film filters," Journal of Quantitative Spectroscopy and Radiative Transfer 198, 179–186 (2017).

8. B. Wu, Z. Liu, G. Liu, X. Liu, P. Tang, G. Du, W. Yuan, and M. Liu, "An ultra-broadband, polarization, and angle-insensitive metamaterial light absorber," J. Phys. D: Appl. Phys. 53, 95106 (2020).

9. S. Mehrabi, M. H. Rezaei, and A. Zarifkar, "Ultra-broadband solar absorber based on multi-layer TiN/TiO 2 structure with near-unity absorption," J. Opt. Soc. Am. B 36, 2602 (2019).

10. L. Chan, E. A. DeCuir, R. Fu, D. E. Morse, and M. J. Gordon, "Biomimetic nanostructures in ZnS and ZnSe provide broadband anti-reflectivity," J. Opt. 19, 114007 (2017).

11. M. Rashid, N. M. Ahmed, N. A. M. Noor, and M. Z. Pakhuruddin, "Silicon quantum dot/black silicon hybrid nanostructure for broadband reflection reduction," Materials Science in Semiconductor Processing 115, 105113 (2020).

12. G. Christidis, U. Koch, E. Poloni, E. D. Leo, B. Cheng, S. M. Koepfli, A. Dorodnyy, F. Bouville, Y. Fedoryshyn, V. Shklover, and J. Leuthold, "Broadband, High-Temperature Stable Reflector for Aerospace Thermal Radiation Protection," ACS applied materials & interfaces 12, 9925–9934 (2020).

13. M. Schürmann, P. J. Jobst, O. Stenzel, S. Wilbrandt, A. Szeghalmi, A. Bingel, P. Munzert, N. Kaiser, and S. Schwinde, “High-reflective coatings for ground and space based applications,” 112 (2014).

14. P. B. Johnson and R. W. Christy, “Optical Constants of the Noble Metals,” (1972).

15. K. Kostarelos and K. S. Novoselov, “Materials science. Exploring the interface of graphene and biology,” Science (New York, N.Y.) 344, 261–263 (2014).

16. Guler, U., Boltasseva, A., & Shalaev, V. M., “Refractory Plasmonics,” Science (New York, N.Y.) 344, 263–264 (2014).

17. C. L. Briant and M. K. Banerjee, “Refractory Metals and Alloys,” (2016).

18. M. A. Keçebaş and K. Şendur, “Enhancing the spectral reflectance of refractory metals by multi-layer optical thin-film coatings,” J. Opt. Soc. Am. B 35, 1845 (2018).

19. C. Hu, J. Liu, J. Wang, Z. Gu, C. Li, Q. Li, Y. Li, S. Zhang, C. Bi, X. Fan, and W. Zheng, “New design for highly durable infrared-reflective coatings,” Light, science & applications 7, 17175 (2018).

20. S. Niu, B. Li, Z. Mu, M. Yang, J. Zhang, Z. Han, and L. Ren, “Excellent Structure-Based Multifunction of Morpho Butterfly Wings: A Review,” J Bionic Eng 12, 170–189 (2015).

21. Y. Zhu, W. Zhang, and Di Zhang, “Fabrication of Sensor Materials Inspired by Butterfly Wings,” Adv. Mater. Technol. 2, 1600209 (2017).

22. Q. Li, Q. Zeng, L. Shi, X. Zhang, and K.-Q. Zhang, “Bio-inspired sensors based on photonic structures of Morpho butterfly wings: a review,” J. Mater. Chem. C 4, 1752–1763 (2016).

23. R. Ahmed, X. Ji, R. M. H. Atta, A. A. Rifat, and H. Butt, “Morpho butterfly-inspired optical diffraction, diffusion, and bio-chemical sensing,” RSC Adv. 8, 27111–27118 (2018).

24. X. Yang, Z. Peng, H. Zuo, T. Shi, and G. Liao, “Using hierarchy architecture of Morpho butterfly scales for chemical sensing: Experiment and modeling,” Sensors and Actuators A: Physical 167, 367–373 (2011).

25. J. He, N. S. Villa, Z. Luo, S. An, Q. Shen, P. Tao, C. Song, J. Wu, T. Deng, and W. Shang, “Integrating plasmonic nanostructures with natural photonic architectures in Pd-modified Morpho butterfly wings for sensitive hydrogen gas sensing,” RSC Adv. 8, 32395–32400 (2018).

26. Y. Zhu, J. Hao, W. Li, J. Yang, and E. Dong, “A new robotic tactile sensor with bio-mimetic structural color inspired by Morpho butterflies,” Bioinspiration & biomimetics 14, 56010 (2019).

27. L. Zhou, J. He, W. Li, P. He, Q. Ye, B. Fu, P. Tao, C. Song, J. Wu, T. Deng, and W. Shang, “Butterfly Wing Hears Sound: Acoustic Detection Using Biophotonic Nanostructure,” Nano Letters 19, 2627–2633 (2019).

28. S. Han, Y. Xu, J. Sun, Y. Liu, Y. Zhao, W. Tao, and R. Chai, “Isolation and analysis of extracellular vesicles in a Morpho butterfly wing-integrated micro vortex biochip,” Biosensors & bioelectronics 154, 112073 (2020).

29. Z. He, A. Elbaz, B. Gao, J. Zhang, E. Su, and Z. Gu, “Disposable Morpho Menelaus Based Flexible Microfluidic and Electronic Sensor for the Diagnosis of Neurodegenerative Disease,” Advanced healthcare materials 7 (2018).

30. M. Kawabe, H. Maeda, and T. Kasuga, “Heat transfer properties of Morpho butterfly wings and the dependence of these properties on the wing surface structure,” RSC Adv. 10, 2786–2790 (2020).

31. Krishna, A., & Lee, J. “Morpho butterfly-inspired spectral emissivity of metallic microstructures for radiative cooling,” Intersociety Conference on Thermal and Thermomechanical Phenomena in Electronic Systems (ITherm) IEEE (2018, May).

32. A. Didari and M. P. Mengüç, “A biomimicry design for nanoscale radiative cooling applications inspired by Morpho didius butterfly,” Scientific reports 8, 16891 (2018).

33. Q. Shen, S. Ma, Z. Luo, S. An, J. He, R. Zhang, P. Tao, C. Song, J. Wu, R. A. Potyrailo, T. Deng, and W. Shang, “Butterfly Wing Inspired High-Performance Infrared Detection with Spectral Selectivity,” Adv. Optical Mater. 8, 1901647 (2020).

34. G. Liao, H. Zuo, Y. Cao, and T. Shi, “Optical properties of the micro/nano structures of Morpho butterfly wing scales,” Sci. China Ser. E-Technol. Sci. 53, 175–181 (2010).

35. Y. Chen, G. Dai, H. Li, H. Xia, S. Ma, J. Gu, and Di Zhang, “Influence of disorders on the optical properties of butterfly wing: Analysis with a finite-difference time-domain method,” Eur. Phys. J. B 86, 2486 (2013).

36. R. H. Siddique, S. Diewald, J. Leuthold, and H. Hölscher, “Theoretical and experimental analysis of the structural pattern responsible for the iridescence of Morpho butterflies,” Optics Express 21, 14351–14361 (2013).

37. M. A. Giraldo, S. Yoshioka, and D. G. Stavenga, “Far-field scattering pattern of differently structured butterfly scales,” Journal of comparative physiology. A Neuroethology, sensory, neural, and behavioral physiology 194, 201–207 (2008).

38. A. Saito, T. Shibuya, M. Yonezawa, M. Akai-Kasaya, and Y. Kuwahara, “Simulation analysis on the optical role of the number of randomly arranged nano-trees on the Morpho butterfly's scale,” 86860J (2013).

39. T. Chen, T. Lu, Z. Chen, W. Wang, W. Zhang, H. Pan, X. Meng, X. Jiang, and S. Zhu, "Microstructures of responsive photonic crystals on the stimuli-responsive performance: Effects and simulation," Sensors and Actuators B: Chemical 305, 127421 (2020).

40. W. Wu, G. Liao, T. Shi, R. Malik, and C. Zeng, "The relationship of selective surrounding response and the nanophotonic structures of Morpho butterfly scales," Microelectronic Engineering 95, 42–48 (2012).

41. K. Chung, S. Yu, C.-J. Heo, J. W. Shim, S.-M. Yang, M. G. Han, H.-S. Lee, Y. Jin, S. Y. Lee, N. Park, and J. H. Shin, "Flexible, angle-independent, structural color reflectors inspired by Morpho butterfly wings," Advanced Materials (Deerfield Beach, Fla.) 24, 2375–2379 (2012).

42. Krishna, Anirudh, et al. "Infrared optical and thermal properties of microstructures in butterfly wings." Proceedings of the National Academy of Sciences 117.3, 1566-1572 (2020)

43. W. Paszkowicz, "Genetic Algorithms, a Nature-Inspired Tool: Survey of Applications in Materials Science and Related Fields," Materials and Manufacturing Processes 24, 174–197 (2009).

44. W. Paszkowicz, "Genetic Algorithms, a Nature-Inspired Tool: A Survey of Applications in Materials Science and Related Fields: Part II," Materials and Manufacturing Processes 28, 708–725 (2013).

45. Tikhonravov, A. V., & Trubetskov, M. K. "Development of the needle optimization technique and new features of OptiLayer design software," In Optical Interference Coatings (Vol. 2253, pp. 10-20). International Society for Optics and Photonics (1994, November).

46. Brian T. Sullivan and J. A. Dobrowolski, "Implementation of a numerical needle method for thin-film design," (1996).

47. S. So, T. Badloe, J. Noh, J. Bravo-Abad, and J. Rho, "Deep learning enabled inverse design in nanophotonics," Nanophotonics 9, 1041–1057 (2020).

48. A. Jiang, Y. Osamu, and L. Chen, "Multilayer optical thin film design with deep Q learning," Scientific reports 10, 12780 (2020).

49. Bendsoe, Martin Philip, and Ole Sigmund. Topology optimization: theory, methods, and applications. Springer Science & Business Media, 2003.

50. Lin, Zin, Benedikt Groever, Federico Capasso, Alejandro W. Rodriguez, and Marko Lončar. "Topology-optimized multilayered metaoptics." Physical Review Applied 9, no. 4 (2018): 044030.

51. Wang, Fengwen, Rasmus Ellebæk Christiansen, Yi Yu, Jesper Mørk, and Ole Sigmund. "Maximizing the quality factor to volume ratio for ultra-small photonic crystal cavities." arXiv preprint arXiv:1810.02417 (2018).

52. Kim, Ganghun, José A. Domínguez-Caballero, and Rajesh Menon. "Design and analysis of multi-wavelength diffractive optics." Optics express 20, no. 3 (2012): 2814-2823.

53. Shokooh-Saremi, Mehrdad, and Robert Magnusson. "Particle swarm optimization and its application to the design of diffraction grating filters." Optics letters 32, no. 8 (2007): 894-896.

54. Zhang, Jiaxin, Sirui Bi, and Guannan Zhang. "A directional Gaussian smoothing optimization method for computational inverse design in nanophotonics." Materials & Design 197 (2021): 109213.

55. Zhang, Jiaxin, Sirui Bi, and Guannan Zhang. "A directional Gaussian smoothing optimization method for computational inverse design in nanophotonics." Materials & Design 197 (2021): 109213.

56. Miller, Owen Dennis. Photonic design: From fundamental solar cell physics to computational inverse design. University of California, Berkeley, 2012.

57. Wang, Jiahui, Yu Shi, Tyler Hughes, Zhexin Zhao, and Shanhui Fan. "Adjoint-based optimization of active nanophotonic devices." Optics express 26, no. 3 (2018): 3236-3248.

58. Hughes, Tyler W., Momchil Minkov, Ian AD Williamson, and Shanhui Fan. "Adjoint method and inverse design for nonlinear nanophotonic devices." ACS Photonics 5, no. 12 (2018): 4781-4787.

59. Yeng, Yi Xiang, Michael Ghebrebrhan, Peter Bermel, Walker R. Chan, John D. Joannopoulos, Marin Soljačić, and Ivan Celanovic. "Enabling high-temperature nanophotonics for energy applications." Proceedings of the National Academy of Sciences 109, no. 7 (2012): 2280-2285.

60. Fu, Sze Ming, Yan Kai Zhong, Nyan Ping Ju, Ming-Hsiang Tu, Bo-Ruei Chen, and Albert Lin. "Broadband polarization-insensitive metamaterial perfect absorbers using topology optimization." IEEE Photonics Journal 8, no. 5 (2016): 1-11.

61. Frandsen, Lars Hagedorn, Anders Harpøth, Peter Ingo Borel, Martin Kristensen, Jakob Søndergaard Jensen, and Ole Sigmund. "Broadband photonic crystal waveguide 60 bend obtained utilizing topology optimization." Optics Express 12, no. 24 (2004): 5916-5921.

62. C. A. Tippets, Y. Fu, A.-M. Jackson, E. U. Donev, and R. Lopez, “Reproduction and optical analysis of Morpho-inspired polymeric nanostructures,” J. Opt. 18, 65105 (2016).

63. F. Zhang, Q. Shen, X. Shi, S. Li, W. Wang, Z. Luo, G. He, P. Zhang, P. Tao, C. Song, W. Zhang, Di Zhang, T. Deng, and W. Shang, “Infrared detection based on the localized modification of Morpho butterfly wings,” Advanced Materials (Deerfield Beach, Fla.) 27, 1077–1082 (2015).

64. Christidis, G., Koch, U., Poloni, E., Leo, E. D., Cheng, B., Koepfli, S. M., ... & Leuthold, J. “Broadband, High-Temperature Stable Reflector for Aerospace Thermal Radiation Protection,” ACS applied materials & interfaces, 12(8), 9925-9934 (2020).

65. Hu, C., Liu, J., Wang, J., Gu, Z., Li, C., Li, Q., ... & Zheng, W. “New design for highly durable infrared-reflective coatings,” Light: Science & Applications, 7(4), 17175-17175 (2018).

66. Yu, K., Fan, T., Lou, S., & Zhang, D. (2013). Biomimetic optical materials: Integration of nature’s design for manipulation of light. Progress in Materials Science, 58(6), 825-873.

67. Goodfellow. (2019, May 08). Titanium Dioxide - Titania (TiO2). AZoM. Retrieved on July 12, 2021 from https://www.azom.com/article.aspx?ArticleID=1179.

68. “FDTD Solutions (Lumerical,2020). https://www.lumerical.com/products/fdtd/”

69. D. R. Smith, D. C. Vier, T. Koschny, and C. M. Soukoulis, “Electromagnetic parameter retrieval from inhomogeneous metamaterials,” Physical review. E, Statistical, nonlinear, and soft matter physics 71, 36617 (2005).

70. B. Razavi and R. Behzad, “RF Microelectronics,” Vol. 1, Prentice Hall, (1998).

71. Palik, Edward D., ed. “Handbook of optical constants of solids.” Vol. 3. Academic Press, (1998).

72. S. Zhang and Y. Chen, “Nanofabrication and coloration study of artificial Morpho butterfly wings with aligned lamellae layers,” Scientific reports 5, 16637 (2015).

73. Macleod, H. A., & Macleod, H. A. (2010). Thin-film optical filters. CRC press.

74. Amin Balazadeh Koucheh, Muhammed Ali Kecebas, and Kursat Sendur. "Impedance mismatch-based enhancement of broadband reflectance of tungsten with bio-inspired multilayers." Journal of Quantitative Spectroscopy and Radiative Transfer 276 (2021): 107899.

75. Kim, Ganghun, José A. Domínguez-Caballero, and Rajesh Menon. "Design and analysis of multi-wavelength diffractive optics." Optics express 20, no. 3 (2012): 2814-2823.

76. Miller, Owen Dennis. Photonic design: From fundamental solar cell physics to computational inverse design. University of California, Berkeley, 2012.

77. Lalau-Keraly, Christopher M., Samarth Bhargava, Owen D. Miller, and Eli Yablonovitch. "Adjoint shape optimization applied to electromagnetic design." Optics express 21, no. 18 (2013): 21693-21701.

78. Kecebas, Muhammed Ali, and Kursat Sendur. "Broadband high-temperature thermal emitter/absorber designed by the adjoint method." JOSA B 38, no. 10 (2021): 3189-3198.

79. Wang, Moran, and Ning Pan. "Predictions of effective physical properties of complex multiphase materials." Materials Science and Engineering: R: Reports 63, no. 1 (2008): 1-30.

80. Choy, Tuck C. Effective medium theory: principles and applications. Vol. 165. Oxford University Press, 2015.